Initial Motor Winding Insulation Lifetime Experimental Results for Electric Aircraft Applications

Thomas Tallerico[1], Aaron D. Anderson[2], Michael Hurrell[3], Jonathan Gutknecht[4], and Mark Valco[5]
NASA Glenn Research Center, Cleveland, OH, 44135, United States

Electric and hybrid-electric aircraft require high-performance and reliable electric motors to meet aviation performance and safety requirements. One of the most common failure mechanisms in electric motors is winding insulation breakdown. In this paper, an initial set of aging experiments are carried out on twisted pairs and motorette specimens. The twisted pairs are aged with multiple steady-temperature thermal aging cycles. The motorette specimens are thermally cycled by applying current to the windings. Partial discharge inception voltage is tracked and reported throughout the aging process. The end goal of this work is to develop methods and models for assessing the lifetime of motor winding insulation in electric and hybrid electric aircraft applications.

I. Introduction

Electric and hybrid electric aircraft must meet the same safety and reliability levels as today's conventional aircraft to gain public acceptance. The reliability of electric and hybrid electric aircraft is heavily dependent on the reliability of their electric motor drivetrains. A NASA sponsored study [1] concluded that current electric motor reliability was not sufficient to enable electric aircraft to meet target industry reliability metrics. As discussed in [2], motor winding insulation breakdown is one of the leading causes of electric motor drivetrain failure; however, models and data sufficient to design high-reliability and high-specific-power electric motors for electric aircraft applications is not available. Specifically, data and models for changes in the partial discharge inception voltage (PDIV) of windings subjected to the thermo-mechanical aging have not been well developed [3]. As was shown in [4] and [5], when electric motors are designed for representative urban air mobility (UAM) missions, winding thermo-mechanical stress will play a significant role in limiting the achievable specific power of a motor.

Recent work, for both automotive and aviation industries, has targeted tracking changes in PDIV with thermal cycling of motorettes. Loubeau et al [6] tracked PDIV of standard motorettes with both constant-temperature thermal aging and thermal cycling. The application of the work was automotive motors. Results show that thermal cycling contributed more significantly to the insulation degradation than constant-temperature aging. Samarakoon et al [7], completed thermal cycling of motorettes targeted towards UAM applications. Preliminary results show degradation of turn-to-turn PDIV with thermal cycling of the motor winding, but issues with specimen manufacturing prevented the collection of phase-to-ground PDIV degradation data. In [8], Mancinelli et al. carried out example qualification of automotive hairpin windings subject to thermal and mechanical stress and found turn-to-turn breakdown of the insulation to occur prematurely due to cracks in the insulation resulting from combined thermo-mechanical aging.

---

[1] Aerospace Research Engineer, Rotating and Drives Systems
[2] Electrical Engineer, Diagnostics and Electromagnetics
[3] Research Mechanical Engineer, Rotating and Drives Systems
[4] Student Trainee, Rotating and Drives Systems
[5] Aerospace Research Engineer, Rotating and Drives Systems

This paper presents a preliminary set of motor winding insulation lifetime experiments targeted towards understanding the thermo-mechanical and thermo-chemical degradation of motor winding PDIV. The end goal of this work is to develop methods and models for characterizing the lifetime of motor winding insulation systems for electric aircraft applications. There are three areas of motor winding insulation considered in this study. First, insulation between different turns of wire within the same coil, referred to as **turn-to-turn** insulation. Second, insulation between different coils within the same slot, referred to as **phase-to-phase** insulation. Third, insulation between coils and the rest of the structure of the motor (the iron core for traditional machines), referred to as **phase-to-ground** insulation. For this preliminary study, building and testing full motors to failure would be impractical. Results for two representative specimen types, twisted pairs and motorettes, are presented here. Twisted pairs consist of two magnet wires twisted together and represent areas where wires are in close proximity, like turn-to-turn insulation and in some cases phase-to-phase insulation. Motorettes consist of a flat iron core with teeth and slots nearly matching the geometry of an actual motor and coils wound around the teeth. Experimental results are presented here for PDIV degradation with constant temperature and thermal cycling aging of twisted pairs and motorettes.

Section II of this paper discusses the partial discharge (PD) experimental setup. Section III presents the constant-temperature aging results for unimpregnated, epoxy-coated, and epoxy-potted twisted wire pairs. Section IV presents the results of initial thermal cycling experiments for motorettes.

II. Partial Discharge Testing Setup and Procedure

PD testing was carried out using the same PD testing setup as was used in [9]. Figure 1 shows the setup graphically. The primary PD measurement system in the setup is a commercial-off-the-shelf PD detecting system developed per IEC 60270 [10]. The system measures PD using a coupling capacitor and measurement impedance, labeled Zm in the figure, in parallel to the test object. The coupling capacitor has a capacitance of 1.3 nF. The measurement instrument processes the voltage signals to detect and record PD pulses. The secondary PD measurement system consists of a high frequency current transformer and an oscilloscope. The current sensor is placed on the ground side of the object under test. The secondary setup is used to confirm that PD detected by the primary setup is real and not system noise, but no direct results from the secondary setup are reported in this paper.

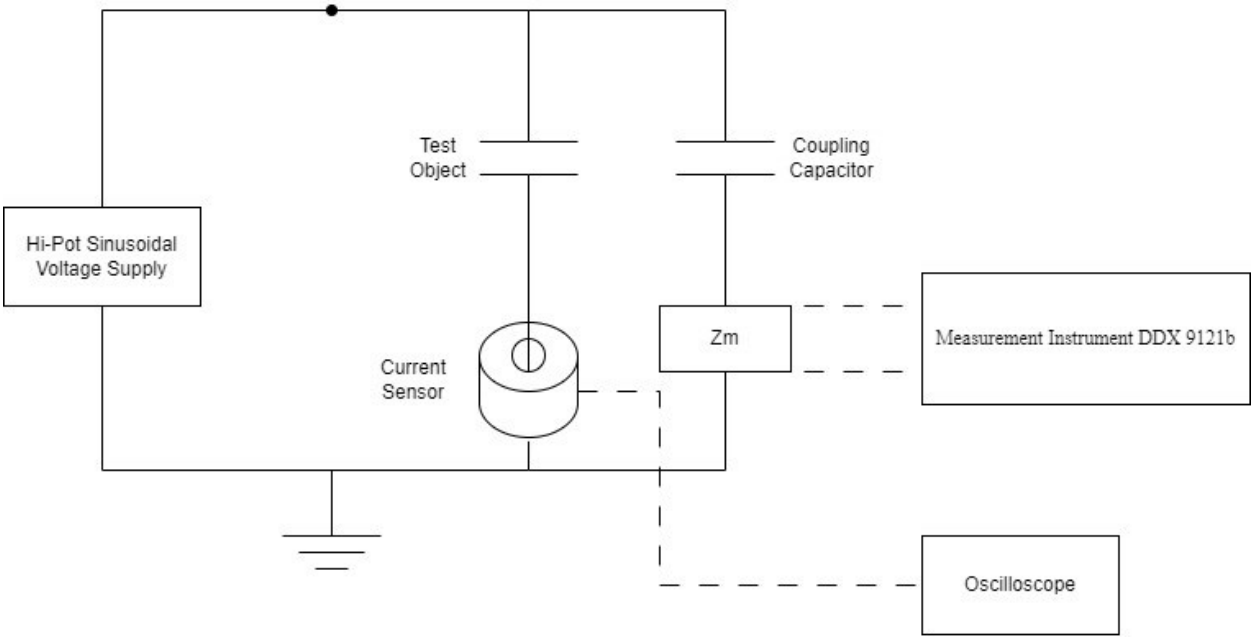

Fig. 1 Partial Discharge Testing Experimental Setup.

A commercial off the shelf hi-pot tester was used to apply voltage to the PD testing circuit. The hi-pot tester was used to detect breakdown of the object under test if it occurs before PD was detected. Breakdown of the insulation in this paper is defined by a 5 mA leakage current. A 60 Hz sinusoidal voltage waveform was used in this testing. As discussed in [2] [3] [11] [12], converter frequencies relevant to aircraft applications will change how the electrical field is distributed in an insulation system as the relative permeability of the insulation components will be different at those frequencies than they are at 60 Hz. 60 Hz waveforms were used in this work due to the unavailability of a

high voltage converter waveform generator. Future efforts plan to incorporate a high voltage converter waveform generator and PDIV testing with converter waveforms.

Voltage was applied to the test circuit at discrete voltage levels for 5 seconds, which is 300 cycles at 60 Hz. One second ramp up and ramp down times were used to reach each test voltage level. The voltage levels used in this testing are provided in Table 1. These voltage levels were selected based on the results of the testing completed in [9] to provide greater resolution around the PDIV of the unimpregnated magnet wire twisted pairs. For all tests, the full 5 second voltage test period was completed regardless of the presence of PD. The number of PD pulses and the peak PD magnitude were recorded with each PDIV measurement. Completing PDIV testing in this manner adds some amount of electrical aging to the test objects. In [9], for an example twisted pair, the authors showed that the number of voltage cycles applied in this PDIV testing did not affect that pair's PDIV. The added electrical aging to the specimens however should still be noted as a possible contributor to the degradation of the specimens' PDIV.

Table 1 Voltage Levels Used in PDIV Measurement Testing.

Voltage Test Levels (V_{rms})						
250	275	300	325	350	375	400
425	450	475	500	525	550	575
600	675	700	725	750	775	800
850	900	950	1000	1050	1100	1200
1300	1400	1500	1600	1700	1800	1900
2000	2100	2200	2300	2400	2500	2750

The PD sensing system monitors the voltage signal across the measurement impedance for impulses that look like PD events. The measurement system records the magnitude of each PD event in terms of the total charge in Coulombs. A PD calibrator was used to calibrate the PD detection system's calculation of PD magnitude for each specimen type by applying known magnitude current pulse across a specimen per IEC 60270 [10].

The voltage supply used in this work produced noise which was registered as low magnitude PD pulses by the PD sensing system. The magnitude of the noise recorded as PD by the sensing system set a noise floor below which real PD could not be recorded. Correspondingly, reducing the noise floor allows for detection of smaller amplitude PD events. To reduce the noise floor of the setup relative to what was reported for the system in [9], the digital band pass filter parameters within the commercial off the shelf PD measurement instrument was shifted to a center of 1300 kHz and a bandwidth of 400 kHz. This change reduced the typical noise floor for a twisted pair test from ~48 pC in [9] to ~21 pC in the testing presented here. The exact noise level depends on both the capacitance of the test specimen and the voltage being output by the voltage source.

For each type of test specimen, the maximum PD charge magnitude of the noise from the voltage source was observed and any PD events at or below that level, with a small margin added, were ignored. For twisted pairs, that threshold was 35 pC. For the motorettes, due to variation in capacitance between different coils and over the course of aging, the noise level was not consistent, so the threshold had to be selected manually for each test.

In addition to noise from the voltage source, there were occasionally other false PD events recorded due to external sources. For instance, static discharge caused by the human operators, or equipment in the room switching on or off causing perturbations in the ground voltage. To avoid these noise sources affecting PDIV measurements, PDIV in this work was defined by a minimum of 5 PD pulses over the full test cycle consisting of ramp up, voltage hold, and ramp down. Only pulses occurring in the first and third quadrant of the voltage waveform were counted.

To ensure the full system was operating correctly, prior to each round of testing 3 steps were taken. First, the PD calibrator was used to set calibrate the PD detector's PD magnitude calculation. Next, noise both with the hi-pot voltage source turned on and off were recorded. Finally, PDIV was measured on a reference unaged and unimpregnated twisted pair specimen. Appendix A provides all calibration and noise level data for the twisted pair testing.

As has been shown in [13], [14], [15], and numerous other publications, PDIV is effected by humidity, pressure, and temperature. All PDIV tests in this paper were carried out at ~600 ft above sea level (elevation of Cleveland Ohio) in a room temperature environment. No attempt was made to monitor or control the humidity of the testing environment. Correspondingly, the reported values are not directly applicable to the PDIV of electric vehicle motors that operate at significantly elevated temperatures and in varying ambient pressures and humidities.

III.Twisted Pair Constant Temperature Aging

Preliminary constant-temperature thermal aging cycles of twisted pair specimens were carried out with the primary goal of capturing the effect of thermo-chemical aging on turn-to-turn insulation PDIV. However, it is not possible to decouple thermo-chemical and thermo-mechanical aging of winding insulation as heating the twisted pairs to temperature results in mechanical stress in the insulation components due to their coefficient of thermal expansion (CTE) mismatch with the copper wire. Additionally, merely forming the twisted pairs results in plastic deformation of the insulation and the copper and corresponding stored residual stress between the magnet wire insulation and the wire itself. As discussed below, the thermal aging cycle count (mechanical stress cycles) and time at temperature are both shown to affect the insulation system.

Three types of magnet wire twisted pair were tested. All specimens are made with 16 AWG magnet wire with heavy build MW-16C polyimide insulation per NEMA 1000 [16]. The twisted pairs were prepared per ASTM D2307 [17]. The three types are:

1. Unimpregnated insulated magnet wire.
2. Epoxy-coated insulated magnet wire.
3. Epoxy-potted insulated magnet wire.

An example of the unimpregnated magnet wire specimens is shown in Figure 3. These twisted pairs have no added epoxy. The coated twisted pairs, shown in Figure 8, only have a light coating of epoxy filling the space between twisted pairs. The coating was applied by brushing the epoxy onto the twisted pairs prior to applying vacuum and pressure to the specimens and curing. The potted twisted pairs, shown in Fig . 13, are incased in a roughly 1 cm thick plate of epoxy.

The intent with these three specimen types was to vary both the thermo-chemical and thermo-mechanical stress environment for the insulation between the twisted pairs. For the thermo-mechanical stress variation, the unimpregnated pairs have only the differential thermal expansion of the polyimide insulation and the copper wire. The coated twisted pairs add the differential expansion of the epoxy to the loading. The potted twisted pairs add additional epoxy and correspondingly more stress due to the differential expansion of the epoxy. Additionally, the potted pairs have a larger thermal mass and are more susceptible to mechanical stresses caused by differential heating and cooling rates through their thickness.

Oxidation is the primary mechanism of thermo-chemical degradation of insulation systems [11]. The unimpregnated twisted pairs directly expose the polyimide insulation to the surrounding environment. The coated twisted pairs put a thin layer of epoxy between the polyimide and the environment similar to the case of the outer end winding of a motor coil. The polyimide is not directly exposed to atmosphere, but the epoxy is itself exposed to the atmosphere. The potted twisted pairs add a thick layer of epoxy between the wires and the atmosphere eliminating direct exposure of the inter-turn insulation to the atmosphere initially. However, in the potted twisted pairs, the higher thermo-mechanical stress led to cracking of the epoxy. In some cases, the cracks in the potted twisted pairs exposed the inter-turn insulation more directly to the ambient environment and the insulation degraded similarly to the coated twisted pairs afterwards.

Groups of twisted pairs were given the three different epoxy treatments and aged at three different temperatures. Table 2 Twisted pair groups names based on insulation type and aging temperature.Table 2 shows the names of each group and the number of samples in each group. The first group was aged at 300 °C to get a large amount of aging on the unimpregnated twisted pairs quickly and inform future tests. No epoxy potted or coated twisted pairs were tested at this temperature as the results in [9] suggested that 300 °C would be too high of a testing temperature for this epoxy. The selection of 270 °C for next group was based on the results in [9] with the goal of applying a large amount of aging to the potted and coated twisted pairs fairly quickly. The final group was aged at 250 °C because the potted twisted pairs saw significant degradation after the first thermal aging cycle at 270 ˚C. Aging at a lower temperature reduces the thermo-mechanical stresses and allows for more resolution in the degradation of PDIV during the initial period of rapid degradation.

Table 2 Twisted pair groups names based on insulation type and aging temperature.

		Insulation type		
		Unimpregnated	**Coated**	**Potted**
Aging Temperature	**300 °C**	300TP		
	270 °C	270TP	270CTP	270PTP
	250 °C	250TP	250CTP	250PTP

The thermal aging cycles were carried out with oven temperature set to the nominal aging temperature. To verify the accuracy of the oven set point, a thermocouple was placed in direct contact with the specimens. When the oven was set to 300 °C, the temperature of the thermocouple typically read around 297.5 °C at steady state. Appendix B contains oven warm up and cool down temperature profiles for the 300 °C aging cycles.

The following sections show the results of each aging groups PDIV degradation with time. Appendix C contains tables with the data from the plots.

A. 300 °C Aging Group results

A total of 13 aging cycles at 300 °C were carried out on this group of samples. The first cycle held the furnace 300 °C temperature set point for 46 hours. The second through sixth held the 300 °C set point for 23 hours each. The remaining seven cycles held the set point for 46 hours each.

Figure 2 shows the changes in measured PDIV for the 300TP specimens over the aging cycles. The PDIV dropped by about 180 V_{rms} on average for the specimens over the aging completed. Steady decay in PDIV is seen with aging. Aging was suspended after 483 hours of time at 300 °C; however, the twisted pairs still have PDIV values greater than the lowest voltages that would be relevant to electric aircraft. Future test for these specimens will continue their thermal aging and/or complete electrical aging at or around their PDIV value.

Figures 3 through 5 show photos of the 300TP samples at different points in the testing. Figure 3 shows 300TP before aging. Figure 4 shows the specimen after the first aging cycle, significant color change is visible. Figure 5 shows 300TP after 7 cycles, minimal color change relative to Figure 4 is visible.

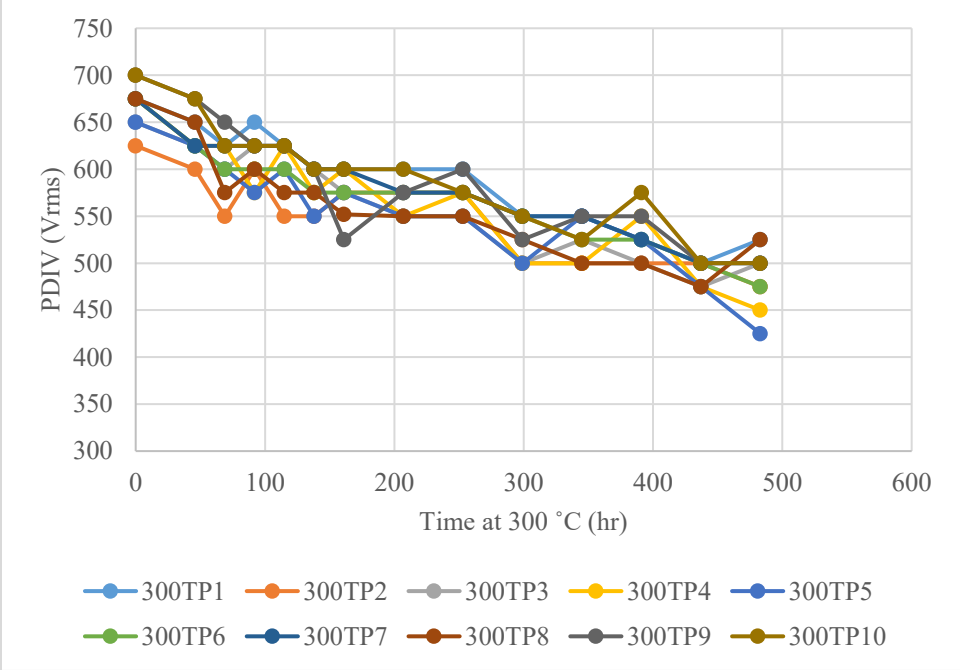

Fig. 2 300TP unimpregnated magnet wire twisted pair PDIV vs time at 300 ˚C oven set point.

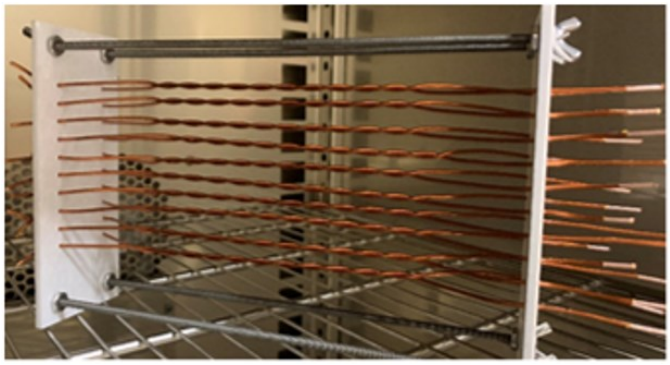

Fig. 3 300TP prior to aging.

Fig. 4 300TP After 1st Thermal Aging Cycle - 46 Hours at 300 ˚C.

Fig. 5 300TP after seven thermal aging cycles and 207 hours at 300 ˚C.

B. 270°C Aging Group

The 270 °C aging group consisted of one set of unimpregnated twisted pairs (270TP), one set of coated twisted pairs (270CTP), and one set of potted twisted pairs (270PTP). Aging was completed with the furnace temperature set point as 270 °C. 270 °C was selected as a temperature to age the potted and coated twisted pairs to a significant level of degradation in a reasonable amount of time. Eleven thermal aging cycles were completed each of which held the furnace set point at 270 °C for 46 hours.

Figure 6 shows the results for the 270TP set. Degradation from an average initial PDIV value of 700 V_{rms} to an average PDIV value of 532 V_{rms} is shown over 500 hours of time at 270°C. This roughly 175 V_{rms} drop in PDIV on average is almost equivalent to the average drop in PDIV experienced by the 300TP set over roughly the same aging time, but at 300 C. As is discussed in Section III-D, one possible explanation for this similar degradation is that the number of aging cycles (thermo-mechanical stress cycles) are roughly equivalent for the two specimen sets.

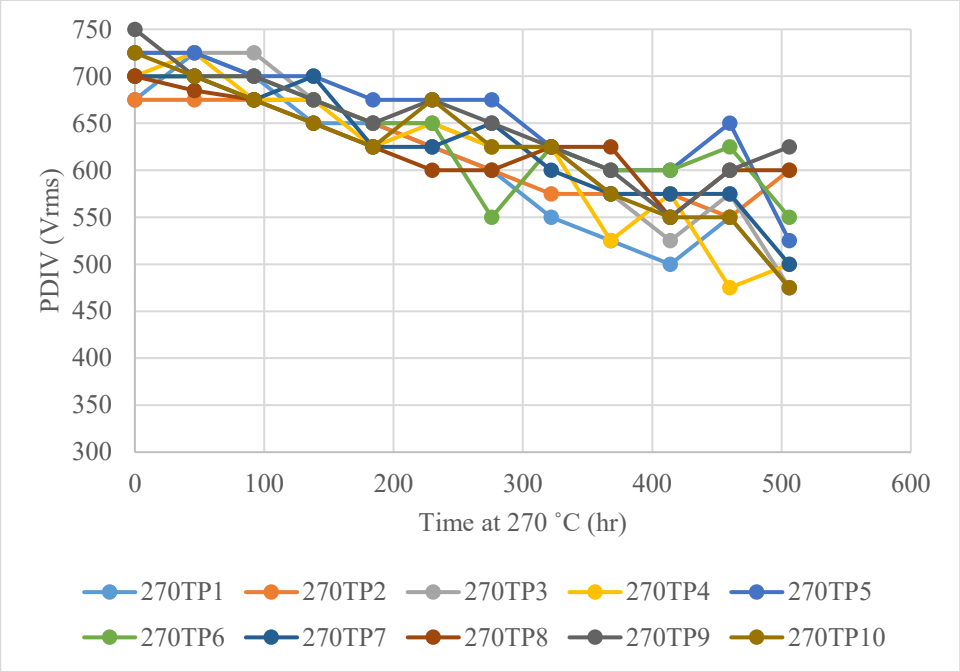

Fig. 6 270°C aging group unimpregnated twisted pairs (270 TP) PDIV vs time at 270 ˚C oven set point.

Figure 7 shows the measured PDIV vs time at 270 °C for the 270CTP set. The average PDIV of the 270TP set vs time at 270 °C is shown as a reference. There is significant variability in the initial PDIV for the 270CTP set due to the relatively uncontrolled manufacturing process of brushing the epoxy onto the twisted pairs. On average, PDIV for the 270CTP set dropped by 482 V_{rms} over the aging cycles completed. The PDIV values of the 270CTP set stay above the PDIV of the 270TP aging set at all times. At 500 hours of time at 270 °C, the 270CTP set PDIV values match that of the initial PDIV values for the 270TP and 300TP unimpregnated twisted pair sets.

Figures 8 through 11 show photos of the 270CTP aging sets at 4 different times during the aging process. Figure 8 shows the 270CTP specimens initially with the grey epoxy and orange magnet wire insulation visible. Figure 9 shows the 270CTP set after a single aging cycle of 46 hours at 270 °C. Both the epoxy and the polyimide magnet wire are shown to have darkened significantly. Figure 10 shows the specimens after 3 aging cycles. The white ceramic filler used in the epoxy has become visible at this stage likely as the epoxy burned away. Figure 11 shows the specimens after all completed aging cycles. At the end of testing relative to after 3 cycles the specimens appear to be slightly whiter in color as more epoxy has baked away leaving more ceramic visible.

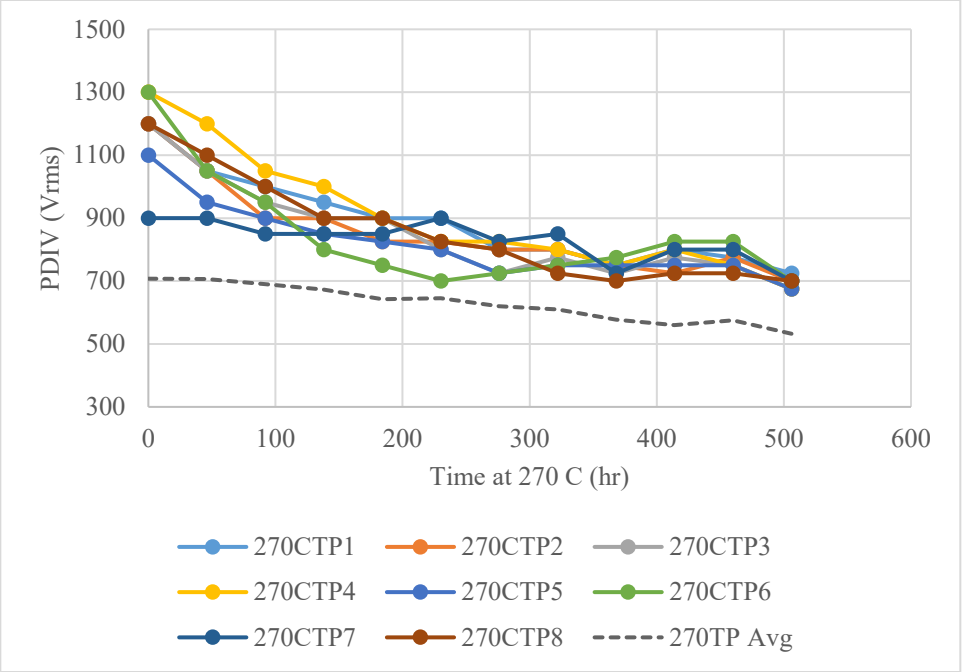

Fig. 7 270 °C aging group coated twisted pairs (270CTP) PDIV vs time at 270 ˚C oven set point.

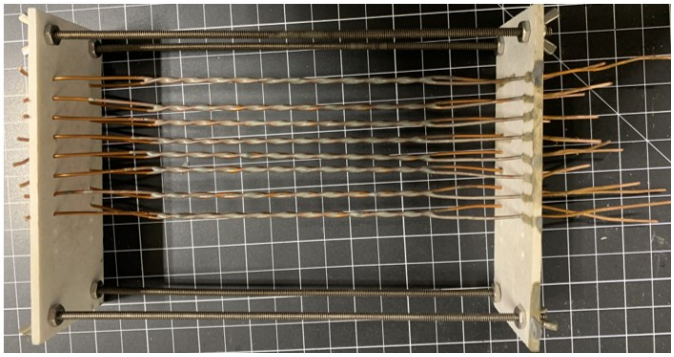

Fig. 8 270CTP prior to aging.

Fig. 9 270CTP after 1 thermal aging cycle.

Fig. 10 270CTP after 3 thermal aging cycles.

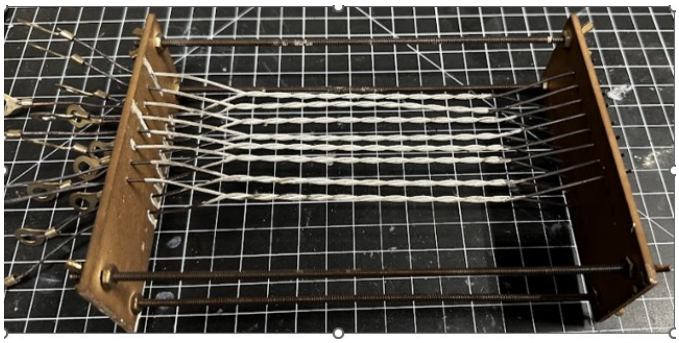

Fig. 11 270CTP after 11 thermal aging cycles.

Figure 12 shows the variation of PDIV with time at 270 ˚C for the 270PTP aging samples. Initial PDIV values again show significant variation, but all initial values are higher than the highest PDIV value recorded for the 270CTP set. Figures 13 through 15 show photos of the potted twisted pairs prior to aging, after the first aging cycle, and after the last aging cycle, respectively.

After the first aging cycle, the 270PTP set had a large average PDIV drop of about 900 V_{rms}, was visually discolored, and had several large cracks, as shown in Figure 14. The large drop in PDIV is likely due to the cracks, since 270CTP samples had a similar discoloration after a single cycle and did not see as large of a drop in PDIV. After the significant drop in PDIV with the first cycle, the specimens exhibited similar behavior to the coated twisted pairs with a steady decay of PDIV occurring with time at temperature. The PDIV values stayed above the average value of the 270TP samples except at one point for 270PTP-7 at roughly 320 hours of time at 270 °C. Similar to the 270CTP, at the end of the cycling the 270PTP set had an average PDIV close to the initial PDIV values for the unimpregnated twisted pair sets (270TP and 300TP). Figure 15 shows the 270PTP to also have appreciable ceramic powder on its surface after the aging was completed.

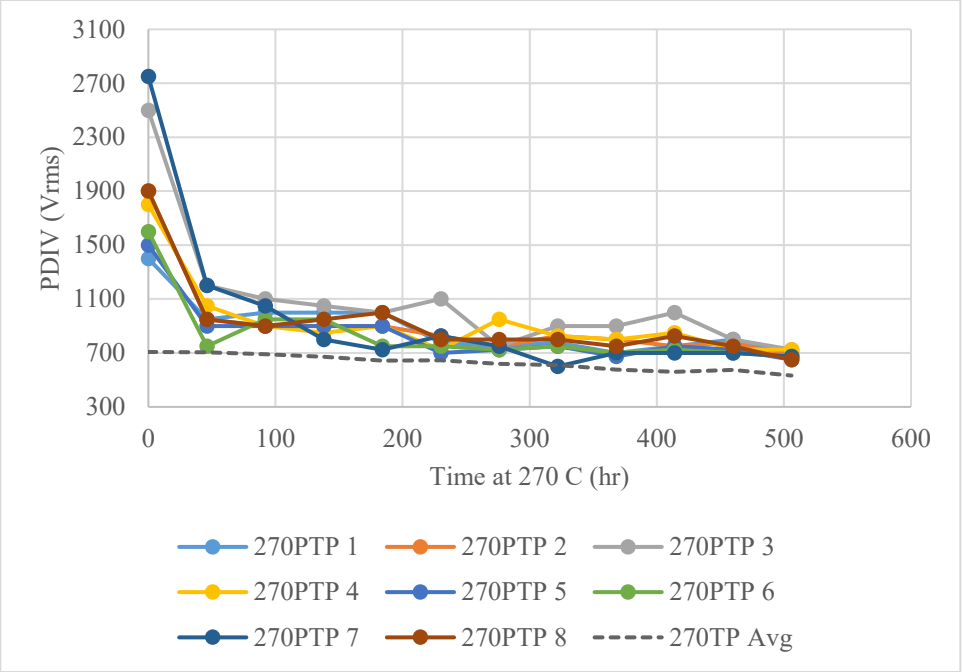

Fig. 12 270 °C aging group potted twisted pair (270PTP) PDIV vs time at 270 ˚C.

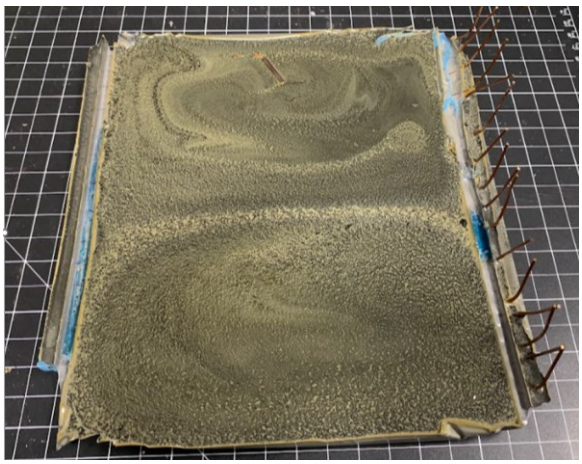

Fig. 13 270PTP prior to aging.

Fig. 14 270PTP after first aging cycle.

Fig. 15 270PTP after last aging cycle.

C. 250 °C Aging Group

The 250 °C aging group consisted of one set of unimpregnated twisted pairs (250TP), one set of coated twisted pairs (250CTP), and one set of potted twisted pairs (250PTP). Aging was completed with the furnace temperature set point as 250 °C. 250 °C was selected for the aging temperature in the hope of slowing down the aging of the potted twisted pairs in order to capture the PDIV changes with time that would have occurred during the initial cycle of the 270PTP. Eight total thermal aging cycles have been completed on the 250 °C aging groups. Cycles 1 through 4 held the 250 °C set point for 23 hours. Cycles 5 and 6 held the 250 °C set point for 46 hours. Cycle 7 held 250 °C set point for 38 hours. No PDIV measurements were made after cycle 7. Cycles 8 and 9 held the 250 °C set point for 46 hours.

Figure 16 shows the PDIV vs time at 250 °C results for the 250TP aging set. The 250TP set was constructed from the same wire type from the same vendor as all other specimens in this paper, but from a different spool. The initial PDIV for this unimpregnated twisted pair set was 50 to 75 V_{rms} below the initial PDIV values of the other unimpregnated twisted pair sets. With the lower aging temperature and less time at temperature completed on these twisted pairs to date, the PDIV has only dropped by 25 to 50 V_{rms}.

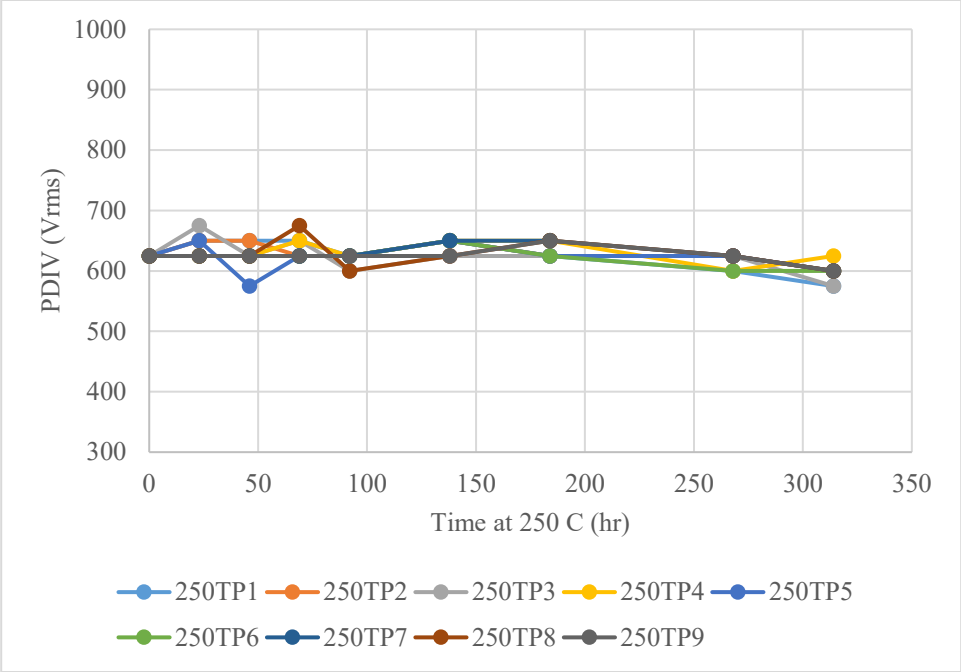

Fig. 16 250 °C aging group twisted pair (250TP) PDIV vs time at 250 ˚C.

Figures 17 and 18 show the 250CTP and 250PTP PDIV vs time at 270 ˚C. Higher initial PDIV values for both the 250CPT and 250PTP are observed relative to the 270CTP and 270PTP sets, reflecting a better epoxy application and potting results for the 250 °C aging group sets. For the 250CPT aging set, significant PDIV degradation is seen for specimens 1 and 3 after the first thermal cycle and for specimen 5 after the second thermal aging cycle. An average total degradation of 1100 V_{rms} has occurred over the 9 thermal cycles.

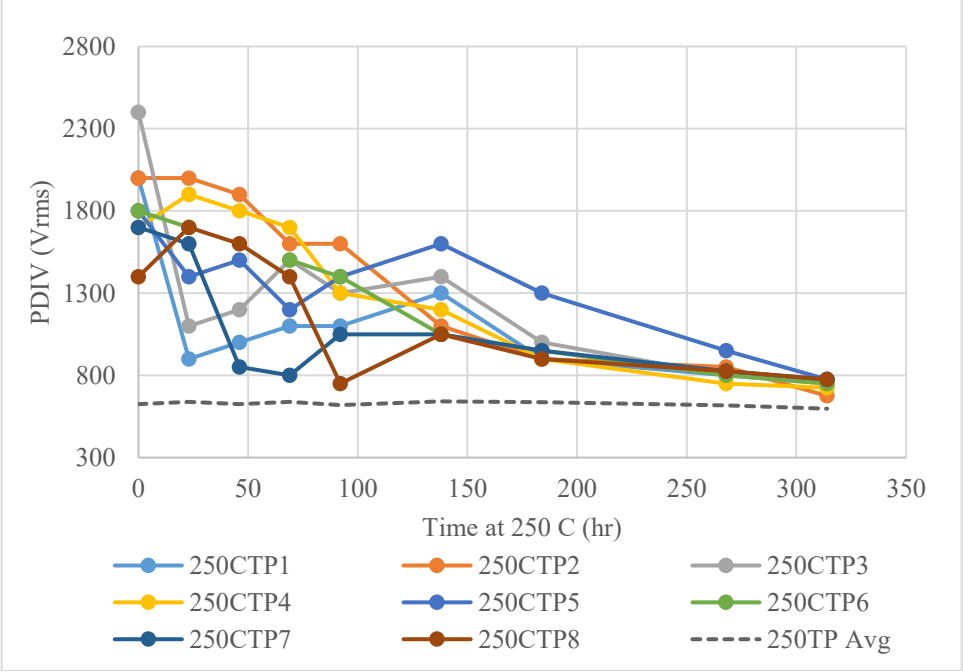

Fig. 17 250 °C aging group coated twisted pair (250CTP) PDIV vs time at 250 ˚C.

For the 250PTP sets in Figure 21, significant variation in degradation of PDIV vs cycles and time at 250 °C is shown. The significant variation in how the specimens degrade can be correlated with where and when cracks in the 250PTP twisted pair epoxy occurred. Figure 19 shows the 250 PTP set initially. Figure 20 shows the specimen after

6 cycles. Cracks are visible in the upper left and lower left corner of the specimen. In Figure 18, the PDIV results after 6 cycles (384 hours of aging) shows that all specimens except 250PTP 3, 4, and 5 have degraded such that their PDIV is less than 1 kV. This result matches with the observed location of the cracks in the epoxy plate in Figure 20.

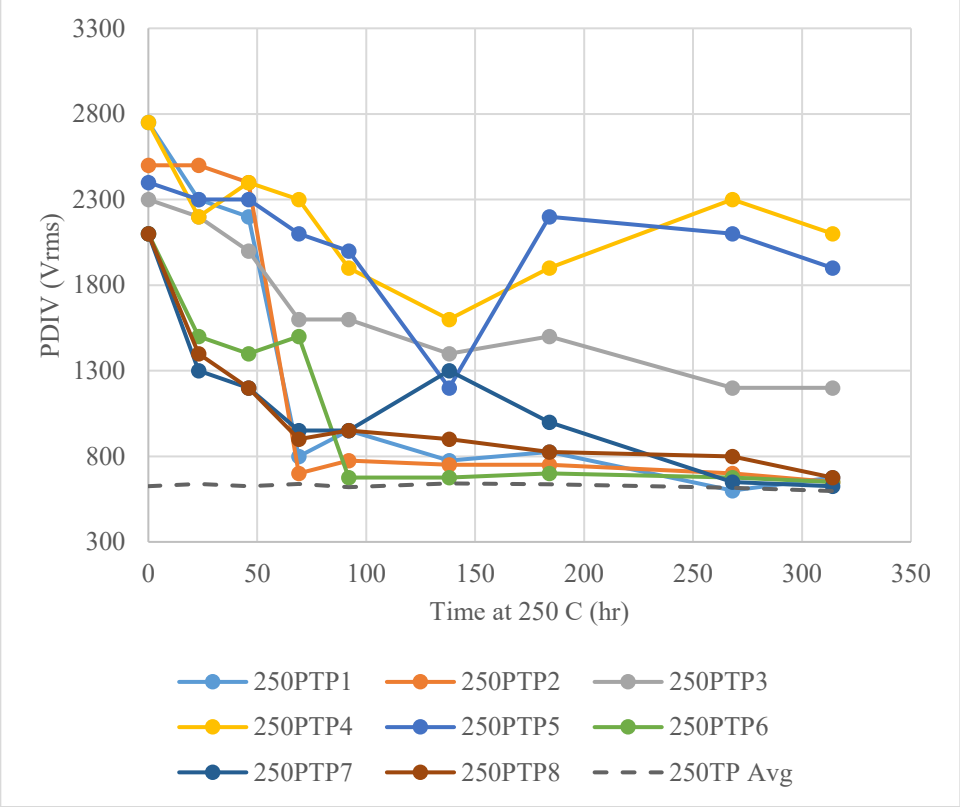

Fig. 18 250 °C aging group potted twisted pair (250PTP) PDIV vs time at 250 ˚C.

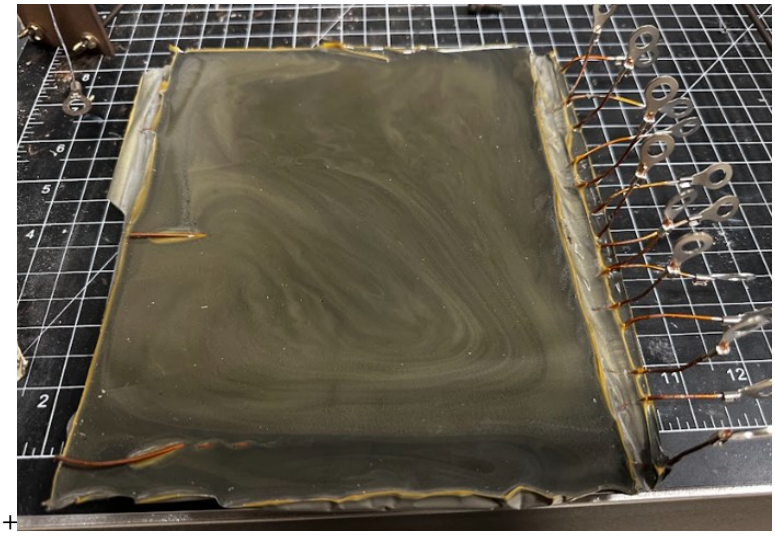

Fig. 19 250PTP prior to aging. Pairs are numbered 1 to 8 from the bottom of the photo to top.

Fig. 20 250PTP after 6 aging cycles. Pairs are numbered 1 to 8 from the top of the photo to bottom.

D. Comparison Across Groups

In this section an estimated equivalent time at 240 °C aging metric is used to normalize the times at temperature to one scale. The estimated equivalent time at 240 °C is calculated assuming the halving rule of thumb approximation for the Arrhenius equation (each 10 °C increase in temperature reduces life by half) [11]. The halving rule is used here as an initial approximation of the Arrhenius equation for these materials. A better fit for the Arrhenius equation for the epoxy and the polyimide will be developed as more data is generated with further testing at lower temperatures. 240 °C is selected for the aging metric, because the polyimide wire insulation is rated for an operational life of 20,000 hours at 240 °C per ASTM D2307 [17]. The equivalent time is calculated by,

$$t_{240} = \int_0^{\tau} 5.96 \times 10^{-8} * \mathrm{e}^{(0.0693*T)} \; dt \tag{1}$$

where t_{240} is the estimated equivalent time at 240 °C, τ is the total time of the experiment, T is the temperature, and t is time.

Figure 21 shows the data for all unimpregnated twisted pairs tested vs estimated equivalent time at 240 ˚C and number of thermal aging cycles. The 300TP set is shown to have been aged past 20,000 hours of equivalent time using this metric and still maintained PDIV above 450 V on average. The 250TP pairs have accumulated minimal equivalent time at 240 °C and show very little degradation. The 270TP set have accumulated 4000 hours of equivalent time at 240 °C and show appreciably more PDIV degradation than the 300TP set at roughly the same amount of estimated equivalent aging time. A possible explanation for the larger drop experienced by the 270TP set relative to the 300TP set over the same estimated aging time is that the 270C aging set took significantly more thermal cycles to get to 4000 hours of equivalent time at 240 °C. The 270TP set average verses number of thermal cycles shows comparable degradation to that experienced by the 300TP set over their first 11 cycles. The 250TP set shows minimal degradation with cycles to date possibly due to the lower temperature used. Whether cycling is playing a significant role in the degradation of the unimpregnated twisted pairs at this time is inconclusive. Subsequent experiments will cycle different groups of twisted pairs to the same temperature but with different times at temperature to study the relative importance of cycles vs time at temperature.

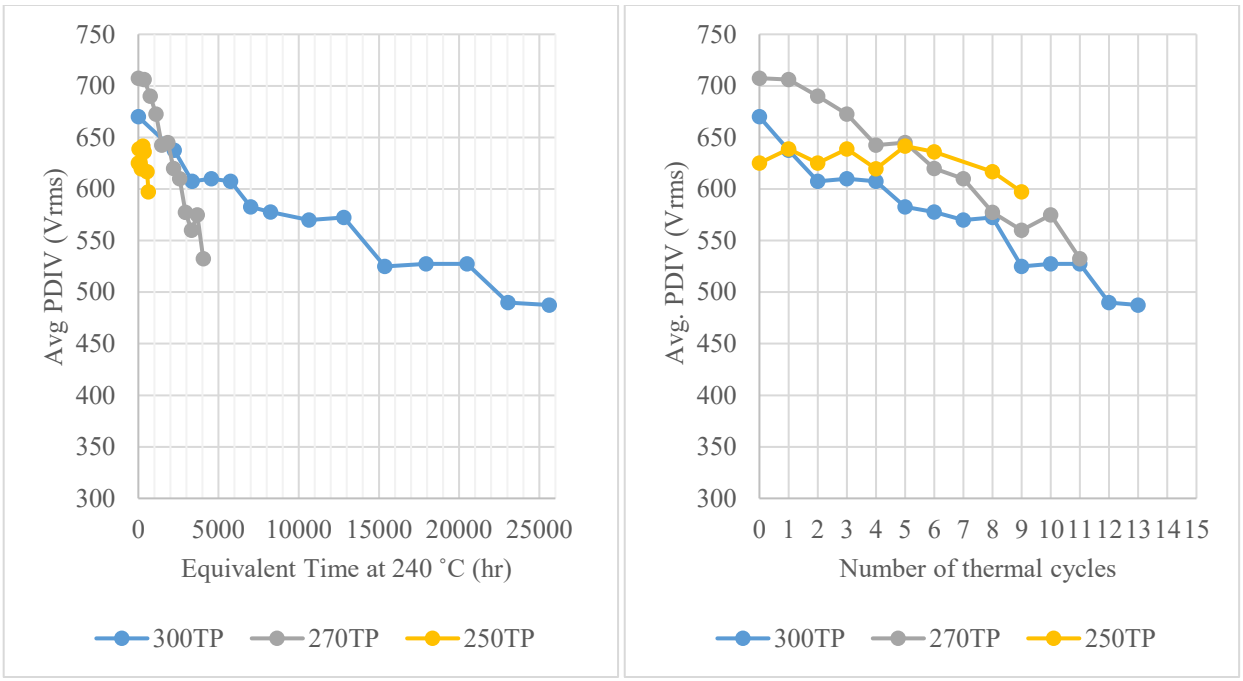

Fig. 21 All unimpregnated twisted pair aging sets average PDIV vs number of thermal cycles.

Figure 22 shows average and minimum PDIV versus estimated equivalent time at 240 °C for both 250 °C and 270 °C coated and potted twisted pairs. Figure 23 show the same PDIV data vs number of thermal aging cycles. The 270PTP set is shown to have similar average and minimum PDIV to that of the 270CTP group after the first cycle. This similarity suggests that after the cracking on the first cycle for the 270PTP group, the 270PTP aged like the coated twisted pairs. Over the first 350 equivalent hours of 240 °C aging, the 270PTP, 250CTP, and 250PTP groups all have similar average PDIV degradation curves over time, although the 270PTP group only has 2 points in that period so the curve is not well resolved. All specimen groups have similar minimum PDIV values after 3 thermal aging cycles. Extracting trends for the dependance of the epoxy aging on temperature from the available data at this time is difficult because the 250 °C and 270 °C groups used different numbers of cycles to reach equivalent levels of thermal aging. Further aging experiments at lower temperatures will use longer cycle times to match the aging points for the 250 °C aging group.

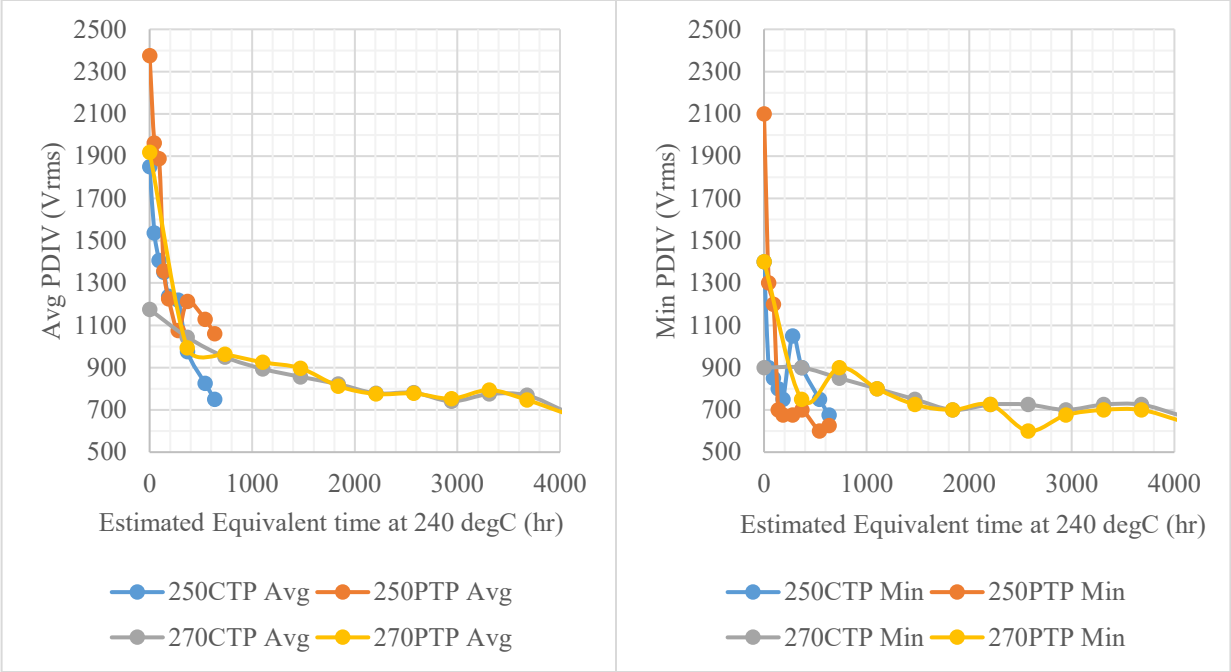

Fig. 22 Average and minimum PDIV for 250 °C and 270 °C coated and potted twisted pair groups vs estimated equivalent aging time at 240 °C.

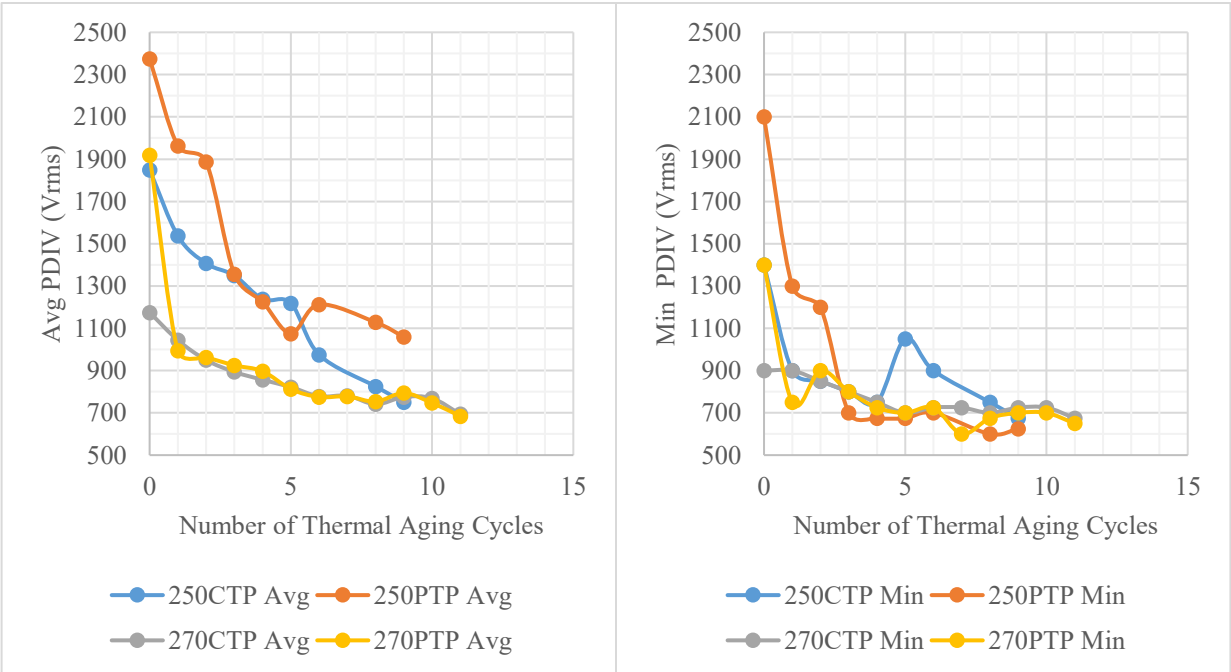

Fig. 23 Average and minimum PDIV for 250°C and 270°C coated and potted twisted pair groups vs number of thermal cycles.

IV. Motorette Thermal Cycling

Thermal cycling of motorettes was carried out to collect an initial data set for the degradation of the insulation system with representative takeoff and climb cycles of an eVTOL UAM mission. Motorette specimens were produced using a representative 100 kW UAM motor geometry designed in [5]. Preliminary aging results for six

motorettes are completed and presented in this paper. Two of the six motorettes tested were wound by an external vendor and were used for preliminary checkout of the thermal cycling experimental setup as described in Appendix D. The other four were wound in-house at NASA. The following sections describe the specimens, the aging setup, and the results for the in-house wound specimens.

A. Description of Specimens

A schematic of the motorettes is shown in Figure 24 and a photo of one motorette prior to potting is in Figure 25. Each motorette consists of 8 concentrated winding coils. The number of coils was selected based on what would fit linearly on a single 12-inch sheet of electrical steel. Low grade M15 electrical steel laminations were used for the motorette cores to minimize cost. The drawing for the motorette core is provided in Appendix E.

Three different PDIV measurements were made on the motorettes as models of different insulation areas in a motor:

1. Voltage applied to one wire in a coil (for example 1A in the figure) while the other wire in the same coil (1B in the figure) is grounded represents **turn-to-turn** voltage stress in a motor. For motorettes with more than two parallel wires, voltage was applied to half the wires while the other half were grounded.
2. Voltage applied to all parallel wire of one coil while all parallel wires of an adjacent coil are grounded represents **phase-to-phase** voltage stress in a motor. Phase-to-phase measurements were only made for the external vendor wound specimens discussed in Appendix D.
3. Voltage applied to all parallel wires of a coil while the iron teeth are grounded represents **phase-to-ground** voltage stress in a motor. Grounding the iron core was accomplished by clamping metal strips to the exposed laminations.

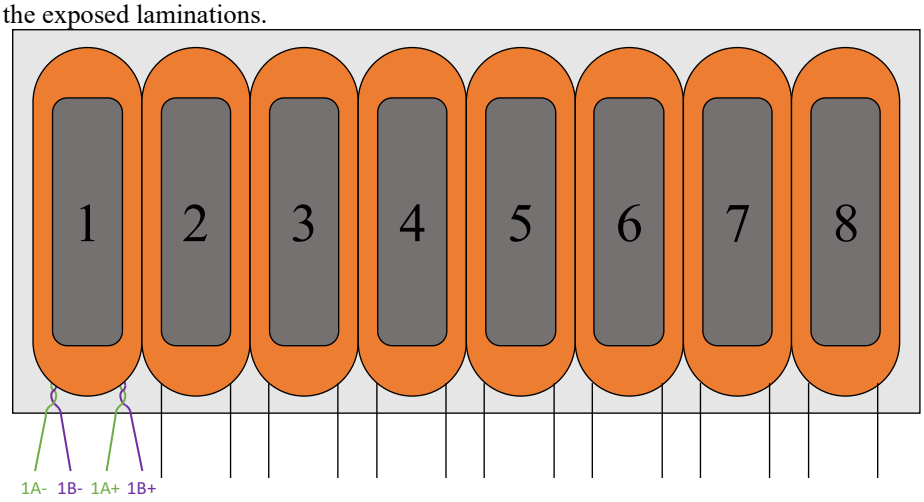

Fig. 24 Motorette schematic. Each of the eight iron teeth is shown in dark gray and numbered. Each coil, shown in orange, is wound around a tooth with two or more wires wound together. Coil 1 is shown with 2 wires in green and purple. For simplicity, all other coils are shown with one black line representing the bundle of wires.

The motorettes are wound with 23 turns of two parallel 16 AWG magnet wires. The magnet wires are heavy build MW-16C wire per [16] matching the twisted pair in Section III. Aramid paper 0.08 mm thick [18] is used for the slot liner insulation between the core and the winding. Two end boards made of carbon fiber-filled 3D printed nylon were placed at each end of the slots and slightly oversized relative to the cores to keep the wires and slot liner from fretting against the core during the winding process. Roughly 40% slot fill is achieved in the specimens. A 1 to 2 mm gap exists between adjacent coils in the slots as the hand winding exceeded expectations. The large gap between phases made phase-to-phase measurements impractical as the only location adjacent phases came into close proximity was on the lead wires. Phase-to-ground and turn-to-turn PDIV were measured for these specimen's coils after each round of thermal cycling. Testing results for these 4 specimens are in Section IV-C.

All motorette specimens were potted in the same epoxy as the twisted pairs. The specimens were cured through the 180 °C post-cure step [19]. The final curing step at 210 °C recommended by the epoxy manufacturer was not completed for the motorette specimens due to temperature limits on the nylon plastic end boards used in the specimens. Figure 26 shows a motorette after potting and prior to aging.

Fig. 25 Motorette prior to potting.

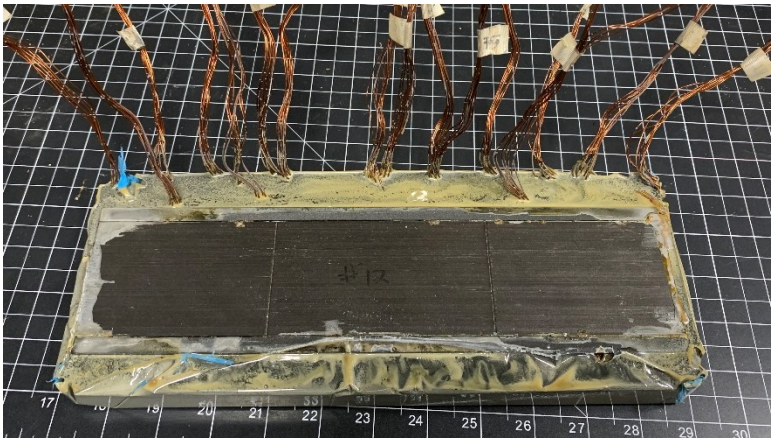

Fig. 26 Example motorette specimen after potting.

B. Thermal Cycling Experimental Setup

Figure 27 shows a graphical representation of the thermal cycle setup. The setup is developed to replicate the setup used to complete similar work in [7]. The motorettes are placed on a cold plate with a thin layer of high thermal conductivity heatsink compound applied between them and the cold plate. The cold plate is supplied with propylene glycol water coolant at 0 °C. Current is supplied to the motorette winding by a low-voltage high-current power supply. Thermocouples are applied to the motorettes on top of their end windings with the heat sink thermal interface compound and taped down with polyimide tape. Thermocouples were not embedded in the coils to avoid any possibility of them effecting the PD measurements. The thermocouple signal was sent to a computer which recorded the cycling data. Heat up cycles were run for set durations of either 3.5 or 5 min with set currents. Set heating cycle durations rather than set max temperatures were chosen to avoid sensitivity to changes in thermal performance of the insulation or a bad thermocouple reading. Additionally, fixed duration cycles more closely match motors' use in aircraft applications where the motor may be asked to do the same mission at the beginning and end of its life. After a heating cycle, all coils in a sample were cooled back to a set minimum temperature (35 °C) before starting the next cycle. Minimum and maximum temperatures and cycle times for each experiment are discussed in the subsequent section.

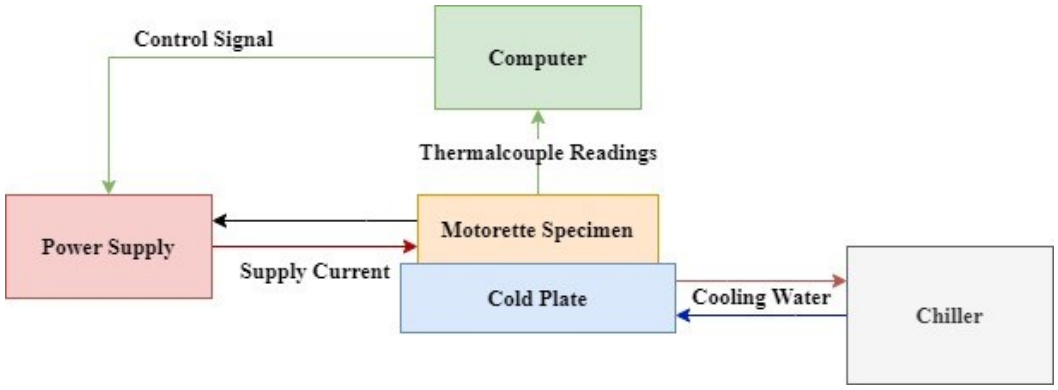

Fig. 27 Diagram of motorette thermal cycling setup.

Based on the limitations of the power supply and the resistance of the coils, the motorettes were cycled with only 4 out of 8 of the coils connected at a time in a 2-series, 2-parallel configuration. For example, as shown in Figure 28, coils 1 and 2 were connected in parallel and then series connected to the parallel connection of coils 3 and 4. This allowed currents of up to 150 A (the power supply current limit) to be used without exceeding the power supply voltage limit. Figure 29 shows representative thermocouple readings from a motorette tested with half the coils powered. Coils 1-3 have similar thermocouple readings while 4 has a lower reading and 5 gets slightly warm. A 2D FEA thermal model, shown in Figure 30, shows a similar temperature distribution. The first half slot and the subsequent three full slots (coils 1-3 and half of coil 4) achieve similar temperature distributions. The middle slot sees some temperature rise, and the last 3 and a half slots see no appreciable increase in temperature.

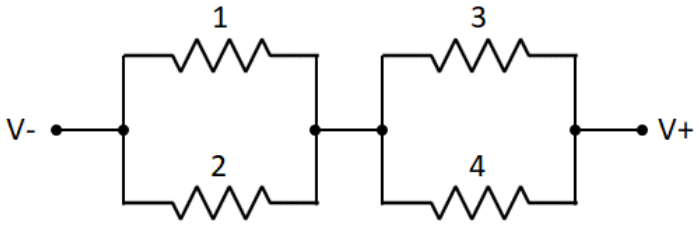

Fig. 28 Winding configuration for motorette testing.

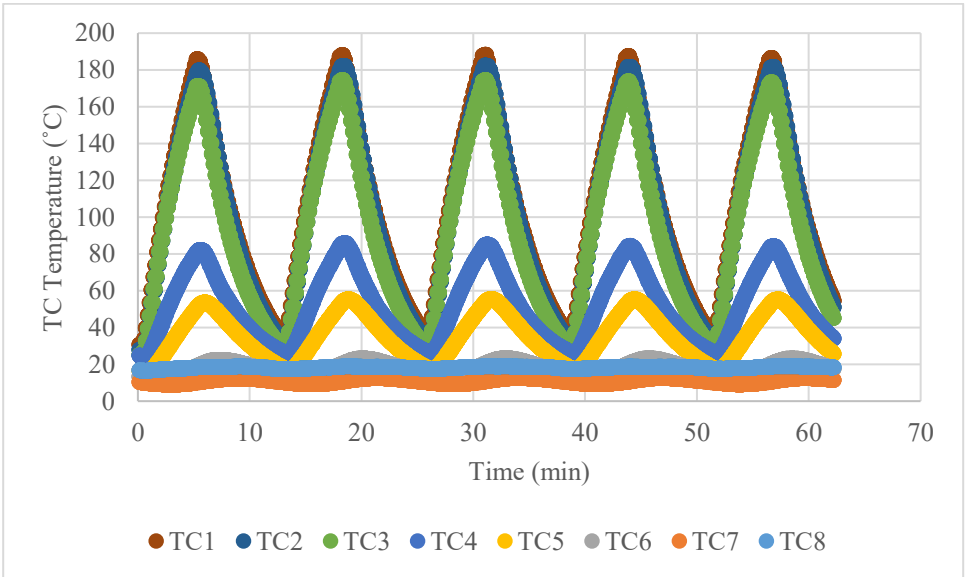

Fig. 29 Example thermocouple data from a motorette with coils 1-4 powered and coils 5-8 unpowered.

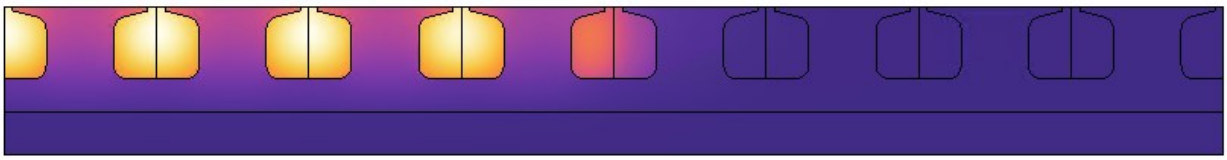

Fig. 30 2D thermal FEA model showing temperature distribution through a cross section of a motorette when only half the windings are powered.

Figure 31 shows accidental additional evidence of the of thermal decoupling between the powered and unpowered windings when cycling half the windings at a time. Motorette 2 experienced an over-temperature event during a round of cycling on coils 1-4. Due to a program error, the coils were not shut down but rather held at high temperature (>250 °C) for ~2 days. Due to the control program error, no thermocouple data was collected during the ~2 days. Coils 1-4 are visibly burned and damaged while coils 5-8 show no color change, providing visual evidence that the powered coils and unpowered coils are fairly well thermally decoupled.

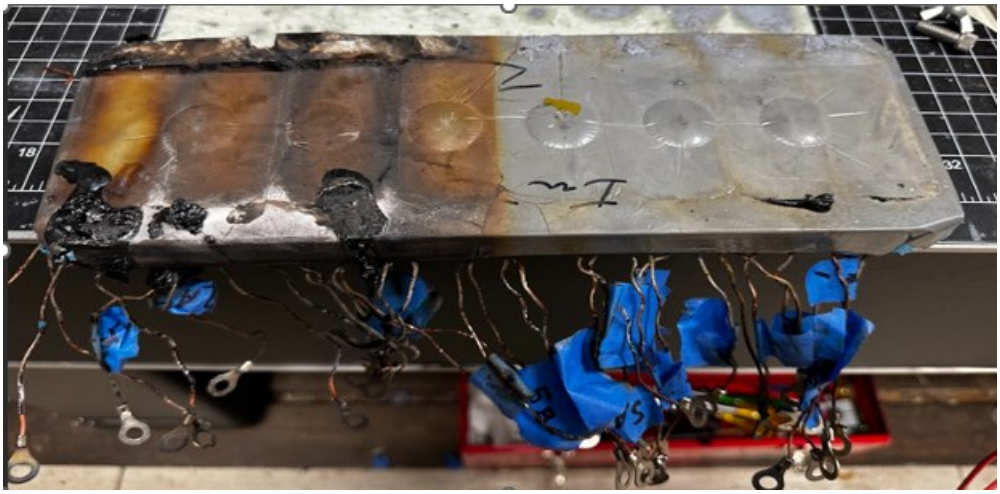

Fig. 31 Motorette number 2 after an accidental ~2 day cycle at >250 °C on coils 1-4. Visual aging of coils 1-4 (left) vs 5-8 (right) provides additional evidence of the lack of thermal coupling between the two halves of the motorette when one half is powered.

PDIV measurements for the motorettes were completed using the PDIV measurement setup discussed in Section II. As mentioned in Section II, the voltage source generates noise that can mask PD events and other noise sources can trigger false PD readings. The higher capacitance and inductance of the motorettes compared to twisted pairs make these effects more pronounced. In addition, there is more variability between motorette coils and more shift in impedances as they age making it more challenging to confidently select an appropriate PD charge threshold. All these factors together introduce a greater level of uncertainty in the motorette results and mitigating them will be the focus of future work.

C. Test Results

Three motorettes were cycled using the thermal cycling setup with cycle durations described in 3. High currents and high peak temperatures were selected to ensure significant degradation occurred within the first 1000 cycles. Future tests will use lower currents and peak temperatures to complete longer duration testing. The fourth motorette was aged for two cycles in the oven at 250 °C with the 250 °C twisted pair aging group. For each of the motorette cycling cases, a 3D FEA model of one quarter of one coil of the motorette was used to simulate the thermo-mechanical cycles experienced by the coils. Details of the model are shown in Appendix F. From the model, estimated hotspot temperature in the winding at every point in time was extracted. Those temperatures were then numerically integrated using Equation 1 to quantify the estimated equivalent 240 °C steady-state temperature aging experienced at the hotspot. Von Mises stress at hotspot (turn-to-turn stress) and Von Mises stress near the iron core

(phase-to-ground stress) in the table were evaluated in the polyimide insulation. The Von-Mises stresses reported are intended as representative numbers for the thermo-mechanical stress in the insulation as there is appreciable difficulty in accurately modeling the geometry of these random wound coils. Table 4 provides a summary of the results from the model.

Table 3 Motorette thermal cycle parameters.

Motorette number	Coil numbers	Current (A_{DC})	Cycle on duration (min)	Threshold temperature for cycle restart (°C)	Peak temperature recorded on thermocouple (°C)
1	1-4	150	3.5	35	190-210
	5-8				
2	1-4	135	5		190-205
	5-8				
3	1-4	130	5		190
	5-8	125	5		18-190

Table 4 3D FEA model estimates of motorette peak temperatures, stresses, and equivalent times at temperature.

Motorette number	Coil numbers	Hotspot Temperature (°C)	Von Misses Stress at Hotspot (MPa)	Von Mises Stress at Ground Wall (MPa)	Equivalent Time at 240 °C Per Cycle	Cycles	Total Equivalent Time at 240 °C
1	1-4	261	56	104	0.029	1603	46.4
	5-8					1197	34.6
2	1-4	236.96	55	88	0.00844	769	6.49
	5-8					504	4.25
3	1-4	218.5	52	78	0.00257	463	1.98
	5-8	200.72	51	63	0.00081	1168	0.95
4	1-8	250	95	90	46.5	2	93

1. Motorette 1 Results

Figures 32 and 33 show the aging results for motorette 1. After cycling, significant PDIV degradation is observed in most measurements. The median turn-to-turn PDIV decreased from 1250 V_{rms} to 550 V_{rms} with every coil decreasing by at least 175 V_{rms}. For the phase-to-ground insulation, half of the coils had insulation breakdown occur and three of the remaining four coils had PDIV decreases. Coils 5-8 had greater degradation in both turn-to-turn and phase-to-ground PDIV than coils 1-4 despite experiencing fewer total cycles. No further cycles were run for motorette after the insulation breakdown was observed during PDIV testing.

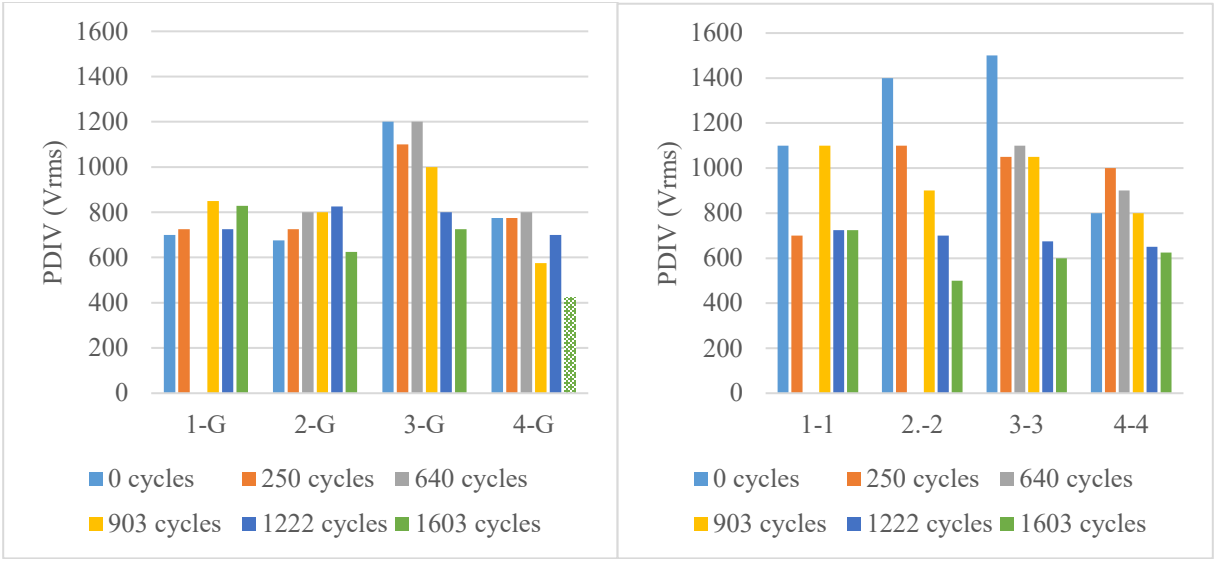

Fig. 32 Motorette 1 coils 1-4 phase-to-ground PDIV measurements (Left) and turn-to-turn PDIV measurements (Right) vs cycles completed of 150 A for 3.5 minutes. Cycle counts listed for each measurement are cumulative. Cross hatched bars signify a breakdown measurement rather than PDIV.

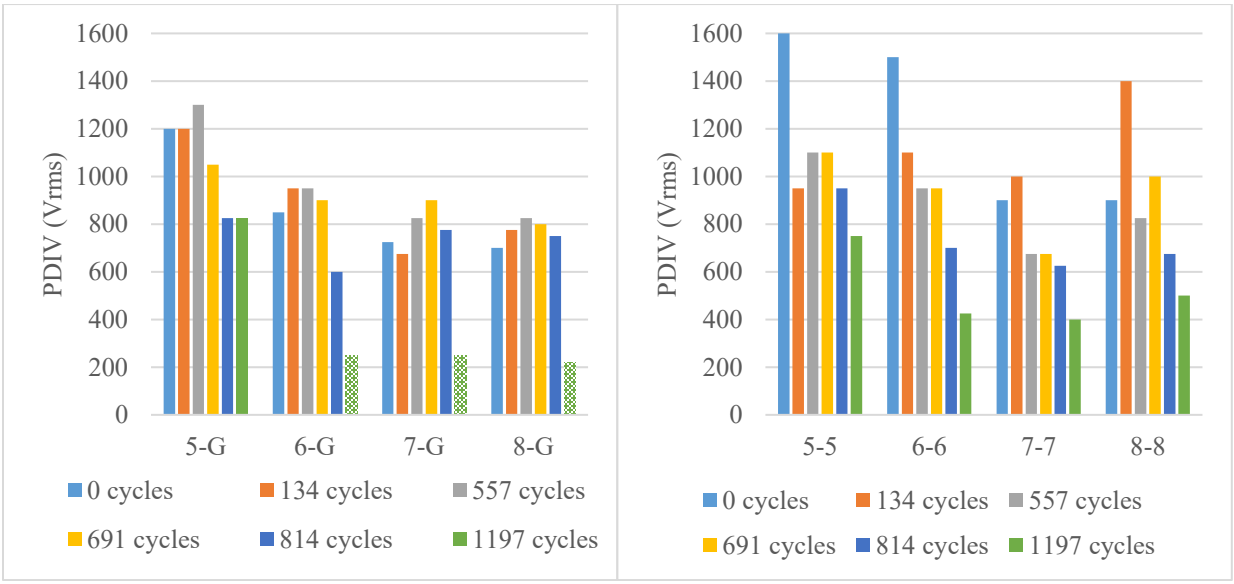

Fig. 33 Motorette 1 coils 5-8 phase-to-ground PDIV measurements (Left) and turn-to-turn PDIV measurements (Right) vs cycles completed of 150 A for 3.5 Min. Cycle counts listed for each measurement are cumulative. Cross hatched bars signify a breakdown measurement rather than PDIV.

2. Motorette 2 Results

Figures 34 and 35 show the PDIV measurements for Motorette 2. Coils 1-4 received 769 cycles while coils 5-8 received 504 cycles. Only one coil had an appreciable decrease in phase-to-ground PDIV with the limited cycles completed for this motorette. Turn-to-turn PDIV trended down for seven out of eight coils with one coil experiencing breakdown. Aging of motorette 2 was suspended at less than 1000 cycles due to the accidental overheating of coils 1-4 as discussed above and shown in Figure 31. The turn-to-turn short in coil 3 may be the root cause of the over-temperature event.

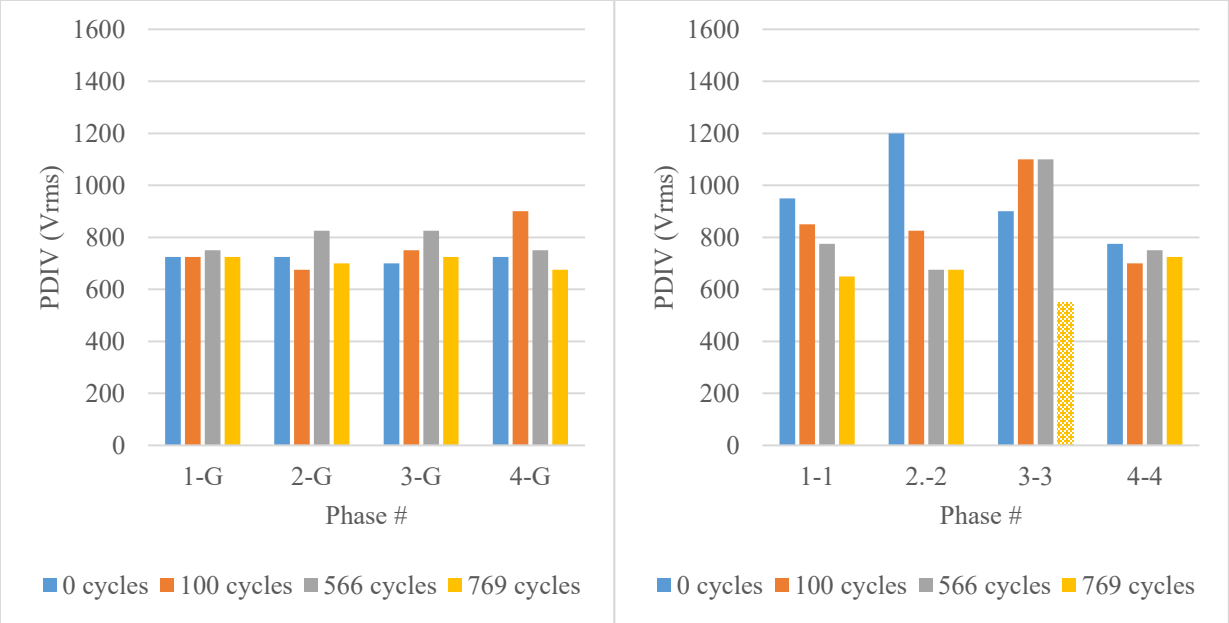

Fig. 34 Motorette 2 coils 1-4 phase-to-ground PDIV measurements (Left) and turn-to-turn PDIV measurements (Right) vs cycles completed of 135 A for 5 min. Cycle counts listed for each measurement are cumulative. Cross hatched bars signify a breakdown measurement rather than PDIV.

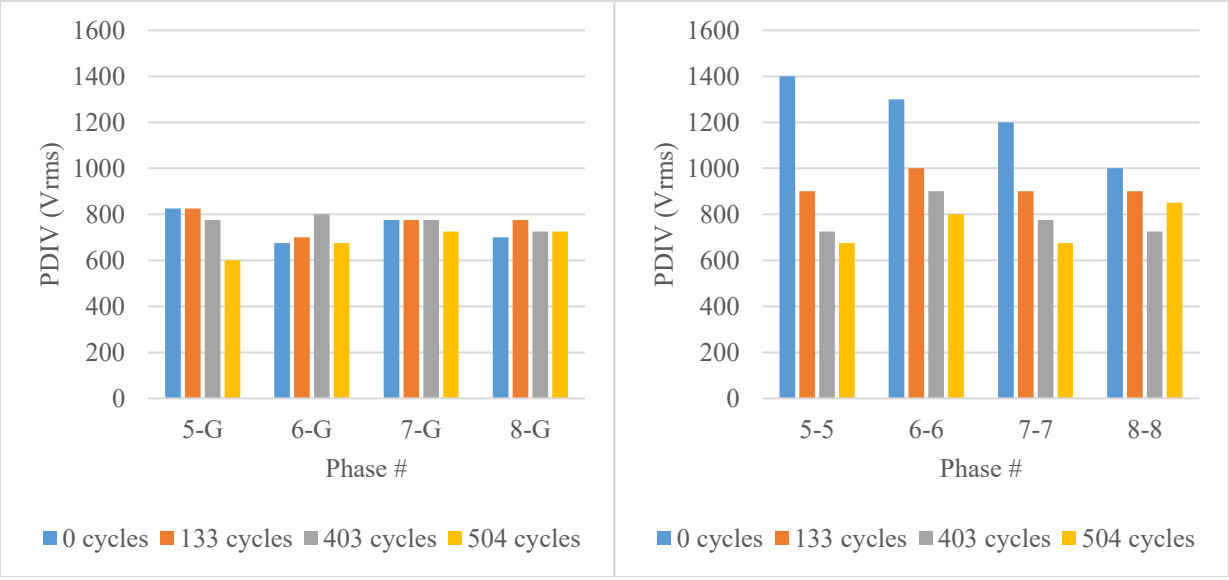

Fig. 35 Motorette 2 coils 5-8 phase-to-ground PDIV measurements (Left) and turn-to-turn PDIV measurements (Right) vs cycles completed of 135 A for 5 min. Cycle counts listed for each measurement are cumulative.

3. Motorette 3, Coil 1 to 4 Results

Figures 36 and 37 show the PDIV measurements for Motorette 3. Coils 1 to 4 received 463 thermal cycles. In three out of four coils, no significant degradation has occurred in the phase-to-ground PDIV insulation over the cycles completed. Coil 2 to ground failed due to breakdown on the first measurement after any cycling, potentially indicating a defect present before any testing was completed. With the exception of coil number 3, all coils' turn-to-turn PDIV is shown to have degraded over the first 463 cycles on coils 1-4 in Figure 36. Coil 3 had a low initial PDIV value, followed by a significant increase in measured PDIV after the first 249 cycles. This result suggests that the initial value measured for coil 3 turn-to-turn PDIV was inaccurate, and the coil is degrading per the subsequent measurements.

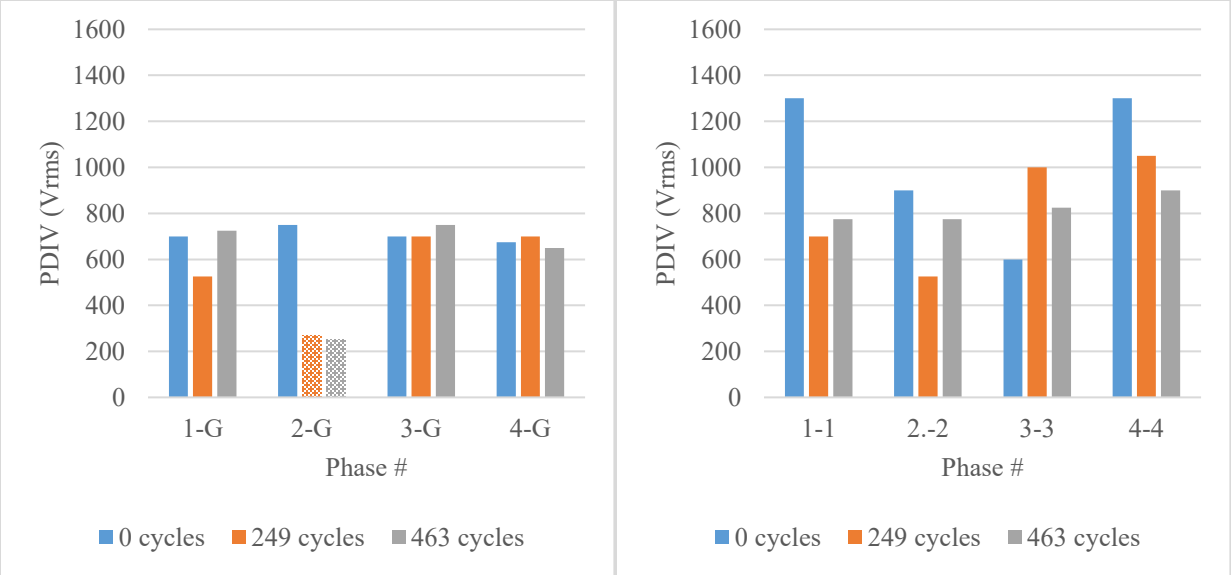

Fig. 36 Motorette 3 Coils 1-4 Phase-to-ground PDIV Measurements (Left) and Turn-to-turn PDIV measurements (Right) Vs cycles completed of 130 A for 5 Min. Cycle counts listed for each measurement are cumulative. Cross hatched bars signify a breakdown measurement rather than PDIV.

4. Motorette 3, Coil 5 to 8 Results

Coils 5-8 received 1168 thermal cycles at lower current than coils 1-4. All coils show degradation in their phase-to-ground insulation. Coil 5, similar to coil 2, failed due to breakdown after the first set of cycles completed. The other three coils showed no degradation after the first 514 cycles but do show significant phase-to-ground PDIV degradation after 1168 cycles.

For turn-to-turn insulation, no degradation in PDIV is observable for coils 6 and 8 through 1168 thermal cycles in Figure 37. Coil 5 shows significant degradation to breakdown of the insulation, but this is believed to result from both parallel wires forming the coil being shorted to ground per the result for coil 5's phase-to-ground insulation.

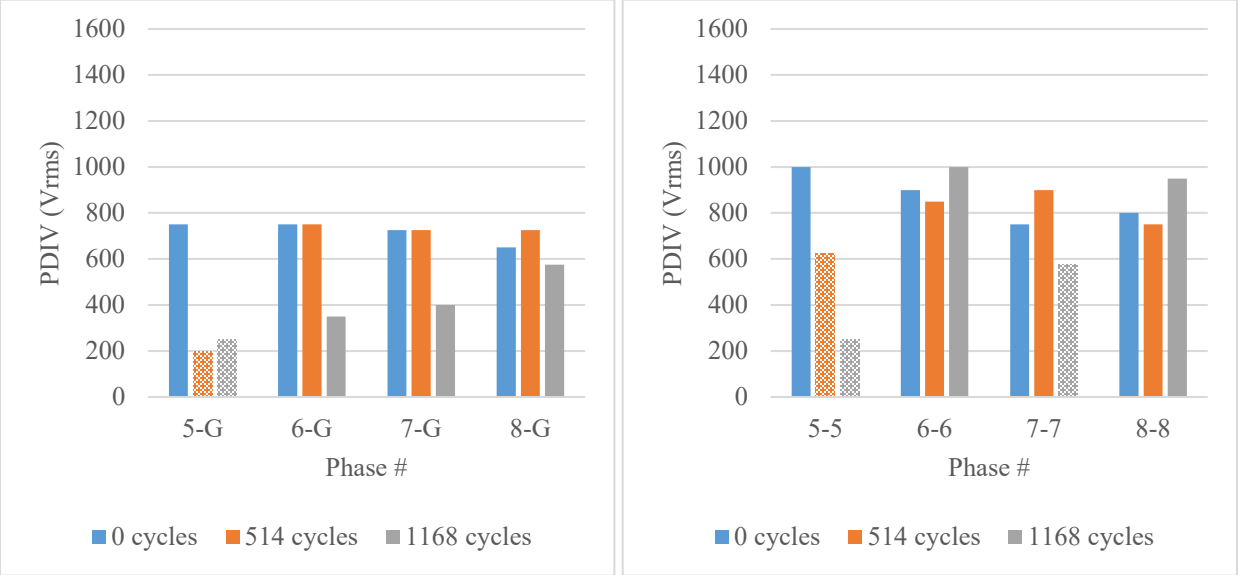

Fig. 37 Motorette 3 Coils 5-8 Phase-to-ground PDIV Measurements (Left) and Turn-to-turn PDIV measurements (Right) Vs cycles completed of 125 A for 5 Min. Cycle counts listed for each measurement are cumulative. Cross hatched bars signify a breakdown measurement rather than PDIV.

5. Motorette 4 Results

Figures 38 and 39, show the phase-to-ground and turn-to-turn PDIV results for Motorette 4. The estimated equivalent time at 240 °C after the first thermal aging cycle is 46.5 hours and after the second cycle is 93 hours. In Figure 38 some phase-to-ground degradation of PDIV is shown; however, no coil experienced breakdown to ground or had a PDIV value measure less than 400 V_{rms}. Similarly, Figure 39 shows overall no trend of degradation in turn-to-turn PDIV.

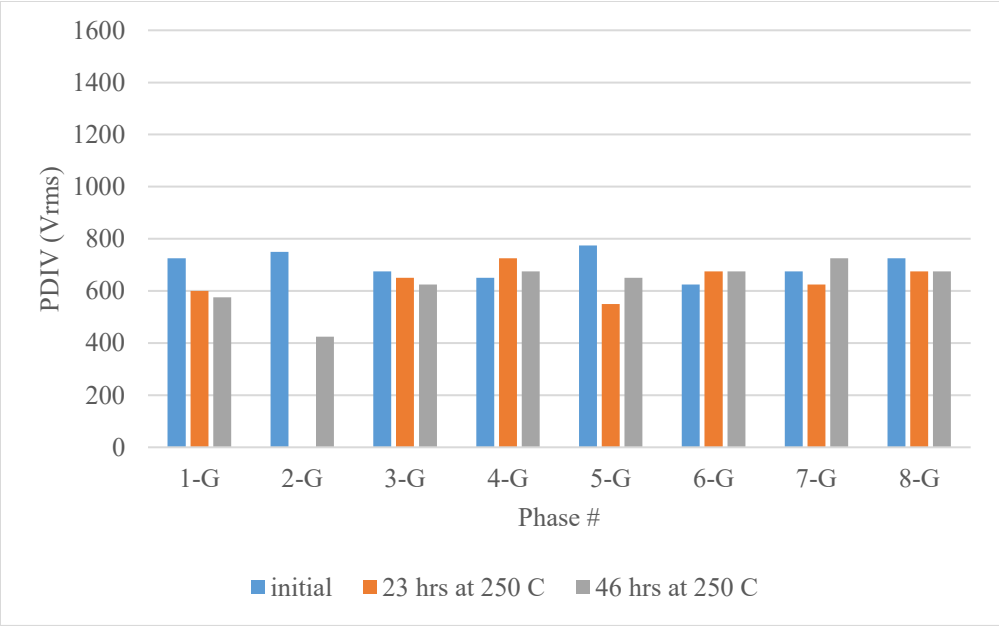

Fig. 38 Motorette 4 phase-to-ground PDIV measurements. Hours at 250°C are cumulative.

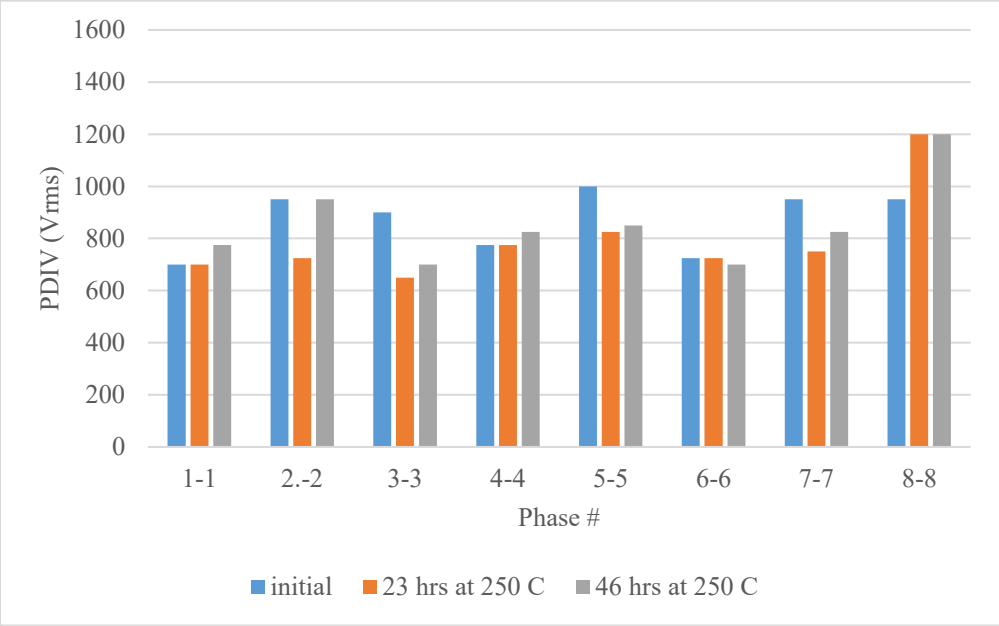

Fig. 39 Motorette 4 turn-to-turn PDIV measurements. Hours at 250°C are cumulative.

6. Comparison Across Motorettes

Motorette 4 had the least degradation in PDIV in both turn-to-turn and phase-to-ground despite receiving more than twice as many hours of 240 °C equivalent aging at the hotspot (93 hours) than any other motorette, indicating that for the cycled motorettes thermo-chemical aging alone is not a significant source of degradation in PDIV.

Figure 40 shows side by side pictures of Motorette 1 and Motorette 4 after all their aging cycles. Motorette 4 is darkened completely indicating appreciable thermo-chemical aging of the full motorette while motorette 1 only has some dark spot in the end windings close to the winding hotspot location. Motorette 4 had the highest modeled Von Misses stress at the hotspot and second highest stress at the ground wall indicating that high stress alone does not immediately degrade the insulation performance.

Among the motorettes aged on the cycling rig, motorette 1 coils and motorette 3 coils 5-8 had significant degradation in phase-to-ground insulation with 5 out of 12 coils shorting. Those motorette coil groups were the ones with cycle counts close to 1000 indicating the approximate lifetime of the ground wall insulation at the temperatures and stress levels used in the experiments. Motorette 1 had the highest modeled Von Misses stress at the ground wall, while motorette 3 coils 5-8 had the lowest stress implying that all other motorettes would be likely to experience ground wall failures if cycled out to greater than 1000 cycles. The resolution of the PDIV testing points does not make it possible to draw a relationship between stress, cycles, and PDIV with the available data. Future work will focus on developing that relationship.

The ground wall insulation of motorettes 1 thru 3 saw very little equivalent time at temperature. The estimated aging times in Table 2 are for the hotspot of the cycling motorette and the temperatures of the ground wall insulation and equivalent aging are significantly less. For example, motorette 1's ground wall insulation had a peak temperature of 220 °C and only experienced 2-4 hours of equivalent time at 240 °C based on the FEA model. Correspondingly, the degradation of their ground wall insulation can be attributed almost entirely to thermo-mechanical effects. The degradation of the ground wall insulation for motorettes 1 and 3 relative to the minimal degradation for motorette 4's ground wall insulation, emphasizes the importance of thermal cycling relative to time at temperature for the degradation of the ground wall insulation.

For turn-to-turn insulation, out of the 24 coils that were thermal cycled on the rig, 22 had PDIV degradation and more than half saw their PDIV drop below 700 V_{rms}. The degradation is more apparent for motorettes 1 and 2 which had higher temperatures and slightly higher model predicted stresses than motorette 3. Only motorette 3 coils 6 and 8 saw no degradation in their PDIV over the thermal cycles completed and they were part of the coil group that saw the lowest temperature and lowest estimated hot spot mechanical stress. Relative to motorette 4 which saw minimal turn-to-turn PDIV degradation and had no coils PDIV drop below 700 V_{rms}, the degradation of the cycled motorette coils point to the relative significance of thermal mechanical cycling for the degradation of the motorettes' turn-to-turn insulation.

Near-term cycling experiments will reduce stress levels on motorettes, attempt to extend cycle counts out past 1000 cycles without breakdown of the insulation, and work to develop relationships between cycles, temperature, stresses, and PDIV.

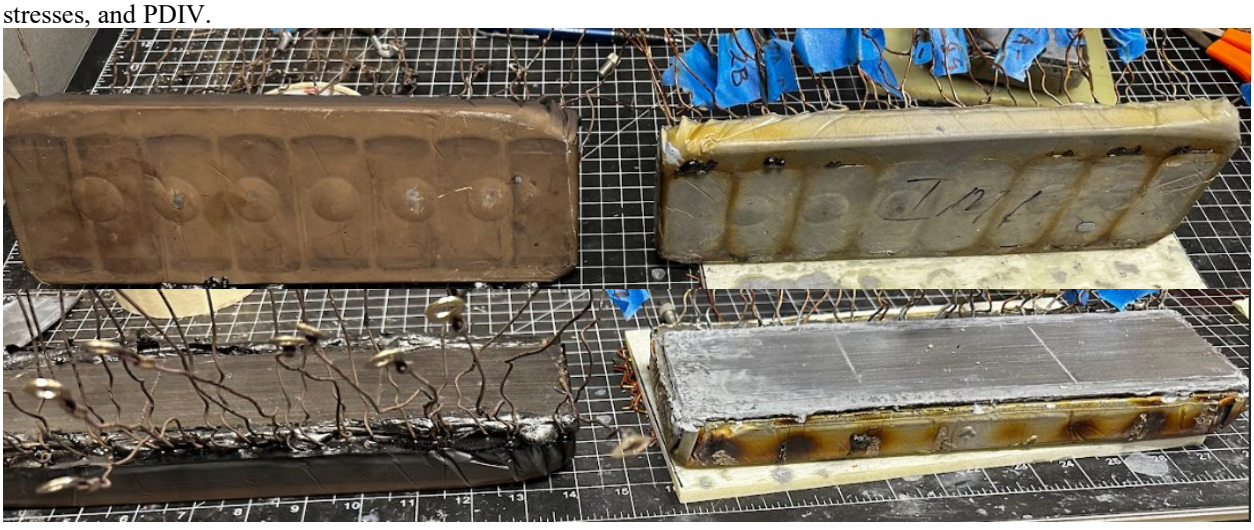

Fig. 40 Motorette 4 (left) and motorette 1 (right) after their aging cycles.

V. Conclusion

In this paper, initial experiments exploring the relationship between thermal cycling and time at temperature for motor insulation degradation were presented. Twisted pairs were aged with long constant-temperature thermal cycles with the intent of showing the impact of thermo-chemical aging. The twisted pairs did show degradation over time at elevated temperatures; however, it is impossible to fully separate thermo-chemical and thermo-mechanical

aging and the degradation also depended on the number of thermal cycles. The effects of thermo-mechanical stress were particularly pronounced in the epoxy potted samples which developed large cracks.

Three motorettes were aged with simulated thermal transient cycles at relevant time scales for electric vertical takeoff and landing aircraft vehicle takeoff and climb mission segments. One motorette was aged with long-duration constant-temperature thermal cycles. The motorette with very few long-duration constant-temperature cycles had very little overall insulation performance degradation. The motorettes that were exposed to simulated takeoff and climb mission segment thermal cycles had significant insulation degradation. The result points to the potential greater importance of thermo-mechanical stress relative to thermo-chemical stress for the lifetime of motors in electric aircraft applications.

The next phase of these experiments will continue to explore the importance of number of cycles, mechanical stress, and time at temperature on insulation degradation. Twisted pair experiments will focus on separating the impact of number of cycles and temperature. Motorette experiments will focus on longer-duration lower-temperature cycling experiments to target thermo-mechanical degradation without any thermo-chemical aging. Additional future work in this area will focus on improving the experimental setups (in particular, reducing the noise in the PD detection setup), incorporating electrical aging with converter frequency waveforms, and extending the testing to other specimen geometries and insulating materials.

Appendix

A. PD System Calibration and Noise Level Data

The following sections contain the noise and calibration information for every round of PD testing completed in this paper. Throughout this section Noise External refers to the noise recorded by the PD detector when the voltage source is powered off. Noise Source is the noise recorded with the voltage source powered on but with the voltage output not active. While actively outputting voltage the noise increases, but the value of that increased noise was not recorded. Calibration is the charge level output by PD calibrator. Ref Specimen is the PDIV of the un-aged reference twisted pair.

Table 5 300 °C unimpregnated twisted pair noise and calibration data.

	Test #	Date	Noise External (pC)	Noise Source (pC)	Calibration (pC)	Ref Specimen (V_{rms})
Testing Completed in Previous Work	0	5/31/2023 - 6/01/2023	1.45	45.60	20	650
	1	6/28/2023	0.66	47.90	20	650
	2	7/3/2023	0.52	48.50	20	650
	3	7/7/2023	0.65	48.2	20	650
	4	7/12/2023	1.41	48.20	20	650
	5	7/14/2023	0.45	48.10	20	650
	6	7/20/2023	0.41	47.50	20	675
	7	7/31/2023	~	47.50	20	675
	8	8/4/2023	~	48.00	20	650
	9	8/9/2023	0.80	~	20	650
	10	8/15/2023	0.80	~	20	675
	11	8/18/2023	~	47.10	20	675
	12	8/24/2023	0.50	47.80	20	675
	13	8/30/2023	0.53	47.50	20	675
	14	9/7/2023	0.75	47.00	20	650
	15	9/14/2023	1.05	47.00	20	650
Testing Completed	16	10/4/2023	~	25.00	20	675
	17	10/13/2023	0.35	25.70	20	625

with 300 kHz center 600 kHz Bandwidth	18	10/16/2023	0.4	27.3	20	650
	19	10/20/2023		27.4	20	675
	20	10/23/2023	0.15	26.6	20	700
	21	10/25/2023	0.22	26.6	20	675
	22	10/27/2023	0.2	26.5	20	675
	23	10/30/2023	0.3	26.9	20	675
	24	11/1/2023	0.35	28	20	700
Testing Completed 1300 kHz Center and 400 kHz Band With	25	3/5/2024	0.28	21.9	20	650
	26	3/8/2024	0.08	21	10	650
	27	3/11/2024	~	21.3	10	675
	28	3/14/2024	~	21.2	10	675
	29	3/19/2024	1.66	20.9	10	650

Table 6 270 °C noise and calibration data. All tests completed with 1300 kHz center frequency and 400 kHz bandwidth.

Test #	Date	Noise Source (pC)	Calibration (pC)	Ref Specimen (V_{rms})
0	3/22/2024	21.5	10	
1	3/25/2024	21	10	700
2	3/28/2024	21.9	10	700
3	4/1/2024	21.2	10	675
4	4/4/2024	21.6	10	700
5	4/9/2024	20.9	10	675
6	4/12/2024	21.2	10	625
7	4/15/2024	21	10	700
8	4/18/2024	20.7	10	650
9	4/22/2024	21.3	10	650
10	4/24/2024	21.5	10	650
11	4/29/2024	20.8	10	650

Table 7 250 °C noise and calibration data. All tests completed with 1300 kHz center frequency and 400 kHz bandwidth.

Test #	Date	Noise External (pC)	Noise Source (pC)	Calibration (pC)	Ref Specimen (V_{rms})
0	5/8/2024		21.1	20	650
1	5/10/2024		22	20	675
2	5/13/2024	1.07	21.3	20	675
3	5/16/2024		21.9	20	650
4	5/20/2024	0.3	22	20	675
5	5/23/2024	0.57	21.1	20	675
6	5/28/2024	0.57	21.1	20	675
7	6/3/2024			20	675
8	6/6/2024	0.15	21.8	10	650

B. Constant Temperature Aging Thermocouple Data

For all constant temperature aging cycles, thermocouple data was recorded using a thermocouple in contact with a specimen being aged. Figure 41 shows all thermocouple data recorded for the constant temperature aging completed at a furnace set point of 300 °C. Note that aging cycles had different durations and correspondingly the time at which cooldown begins is different for each aging cycle. The measured TC temperature was typically 2-3 °C below the set point.

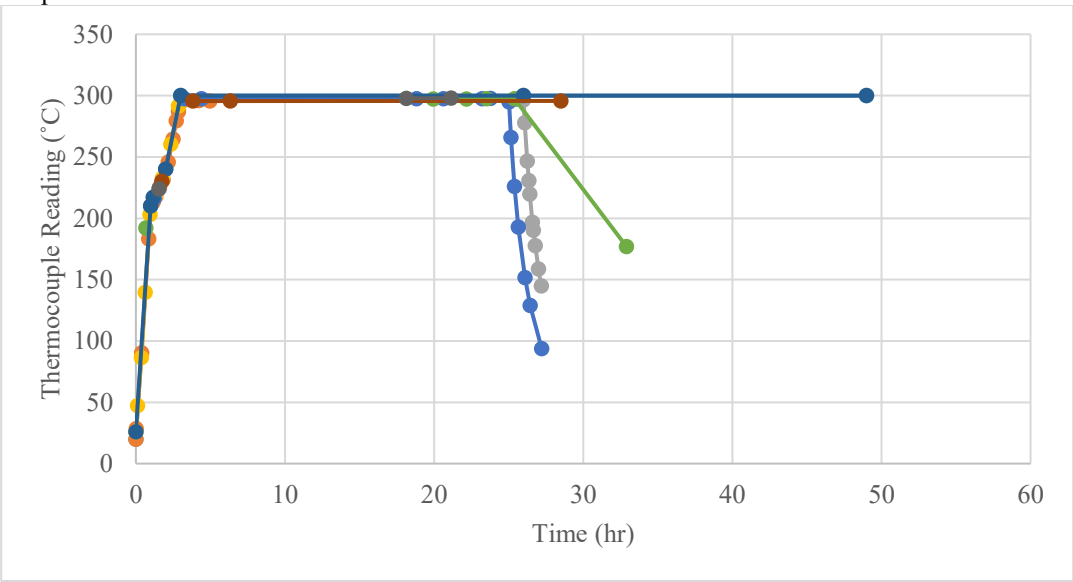

Fig. 41 Recorded thermocouple temperature data points from 300 °C constant temperature aging.

C. Twisted Pair PDIV Data Tables

Table 8 300 °C unimpregnated twisted pair data.

Test #	Date	time at 300 C (hr)	Equivalent time at 240 C (hr)	PDIV (Vrms)											
				300TP1	300TP2	300TP3	300TP4	300TP5	300TP6	300TP7	300TP8	300TP9	300TP10	Avg	Min
0	10/4/2023	0	0	675	625	650	675	650	675	675	675	700	700	670	625
1	10/13/2023	46	2234	650	600	625	625	625	625	625	650	675	675	670	625
2	10/16/2023	69	3351	625	550	600	625	600	600	625	575	650	625	670	625
3	10/20/2023	92	4555	650	600	625	575	575	600	625	600	625	625	670	625
4	10/23/2025	115	5759	625	550	625	625	600	600	625	575	625	625	670	625
5	10/25/2023	138	7005	600	550	600	575	550	575	600	575	600	600	670	625
6	10/27/2023	161	8252	600	575	575	600	575	575	600	552	525	600	670	625
7	10/30/2023	207	10644	600	575	550	550	550	575	575	550	575	600	670	625
8	11/1/2023	253	12822	600	575	550	575	550	575	575	550	600	575	670	625
9	3/5/2024	299	15368	550	500	500	500	500	550	550	525	525	550	670	625
10	3/8/2024	345	17931	550	500	525	500	550	525	550	500	550	525	670	625
11	3/11/2024	391	20494	525	500	500	550	525	525	525	500	550	575	670	625
12	3/14/2024	437	23057	500	500	475	475	475	500	500	475	500	500	670	625
13	3/19/2024	483	25620	525	475	500	450	425	475	500	525	500	500	670	625

Table 9 270 °C unimpregnated twisted pair data.

Test #	Date	Time at 270 (hr)	Equivalent Time at 240 C (hr)	PDIV (Vrms)											
				270TP1	270TP2	270TP3	270TP4	270TP5	270TP6	270TP7	270TP8	270TP9	270TP10	Avg	Min
0	3/22/2024	0	0.00	675	675	725	700	725	700	700	700	750	725	707.5	675
1	3/25/2024	46	367.75	725	675	725	725	725	700	700	685	700	700	706	675
2	3/28/2024	92	735.50	700	675	725	675	700	700	675	675	700	675	690	675
3	4/1/2024	138	1103.25	650	675	675	675	700	675	700	650	675	650	672.5	650
4	4/4/2024	184	1471.00	650	650	650	625	675	650	625	625	650	625	642.5	625
5	4/9/2024	230	1838.75	625	625	650	650	675	650	625	600	675	675	645	600
6	4/12/2024	276	2206.50	600	600	625	625	675	550	650	600	650	625	620	550
7	4/15/2024	322	2574.25	550	575	625	625	625	625	600	625	625	625	610	550
8	4/18/2024	368	2942.00	525	575	575	525	600	600	575	625	600	575	577.5	525
9	4/22/2024	414	3309.75	500	575	525	575	600	600	575	550	550	550	560	500
10	4/24/2024	460	3677.50	550	550	575	475	650	625	575	600	600	550	575	475
11	4/29/2024	506	4045.25	475	600	475	500	525	550	500	600	625	475	532.5	475

Table 10 270 °C coated twisted pair data.

Test #	Date	Time at 270 (hr)	Equivalent Time at 240 C (hr)	PDIV (Vrms)									
				279CTP1	279CTP2	279CTP3	279CTP4	279CTP5	279CTP6	279CTP7	279CTP8	Avg	Min
0	3/22/2024	0.00	0	1200	1200	1200	1300	1100	1300	900	1200	1175	900
1	3/25/2024	46.00	368	1050	1050	1050	1200	950	1050	900	1100	1044	900
2	3/28/2024	92.00	736	1000	900	950	1050	900	950	850	1000	950	850
3	4/1/2024	138.00	1103	950	900	900	1000	850	800	850	900	894	800
4	4/4/2024	184.00	1471	900	825	900	900	825	750	850	900	856	750
5	4/9/2024	230.00	1839	900	825	800	825	800	700	900	825	822	700
6	4/12/2024	276.00	2207	800	800	725	825	725	725	825	800	778	725
7	4/15/2024	322.00	2574	800	800	775	800	750	750	850	725	781	725
8	4/18/2024	368.00	2942	750	750	725	750	750	775	725	700	741	700
9	4/22/2024	414.00	3310	800	725	775	800	750	825	800	725	775	725
10	4/24/2024	460.00	3678	775	775	750	750	750	825	800	725	769	725
11	4/29/2024	506.00	4045	725	700	675	675	675	700	700	700	694	675

Table 11 270 °C potted twisted pair data.

Test #	Date	Time at 270 (hr)	Equivalent Time at 240 C (hr)	PDIV (Vrms)									
				270PTP 1	270PTP 2	270PTP 3	270PTP 4	270PTP 5	270PTP 6	270PTP 7	270PTP 8	Avg	Min
0	3/22/2024	0	0	1400	1900	2500	1800	1500	1600	2750	1900	1919	1400
1	3/25/2024	46	368	950	950	1200	1050	900	750	1200	950	994	750
2	3/28/2024	92	736	1000	900	1100	900	900	950	1050	900	963	900
3	4/1/2024	138	1103	1000	900	1050	850	900	950	800	950	925	800
4	4/4/2024	184	1471	1000	900	1000	900	900	750	725	1000	897	725
5	4/9/2024	230	1839	775	825	1100	725	700	750	825	800	813	700
6	4/12/2024	276	2207	750	750	750	950	725	725	750	800	775	725
7	4/15/2024	322	2574	775	825	900	825	750	750	600	800	778	600
8	4/18/2024	368	2942	700	800	900	800	675	700	700	750	753	675
9	4/22/2024	414	3310	750	750	1000	850	750	725	700	825	794	700
10	4/24/2024	460	3678	800	775	800	725	725	700	700	750	747	700
11	4/29/2024	506	4045	700	675	725	725	650	675	675	650	684	650

Table 12 250 °C unimpregnated twisted pair data.

Test #	Date	Time at 250 (hr)	Equivalent Time at 240 C (hr)	PDIV (Vrms)										
				250TP1	250TP2	250TP3	250TP4	250TP5	250TP6	250TP7	250TP8	250TP9	Avg	Min
0	5/8/2024	0	0	625	625	625	625	625	625	625	625	625	625	625
1	5/10/2024	23	47	650	650	675	625	650	625	625	625	625	639	625
2	5/13/2024	46	93	650	650	625	625	575	625	625	625	625	625	625
3	5/16/2024	69	140	650	625	650	650	625	625	625	675	625	639	625
4	5/20/2024	92	186	625	625	600	625	625	625	625	600	625	619	625
5	5/23/2024	138	278	650	650	625	650	650	650	650	625	625	642	625
6	5/28/2024	184	371	625	625	625	650	625	625	650	650	650	636	625
7	6/3/2024	268	542	600	625	625	600	625	600	625	625	625	617	625
8	6/6/2024	314	634	575	600	575	625	600	600	600	600	600	597	625

Table 13 250 °C coated twisted pair data.

Test #	Date	Time at 250 (hr)	Equivalent Time at 240 C (hr)	PDIV (Vrms)									
				250CTP1	250CTP2	250CTP3	250CTP4	250CTP5	250CTP6	250CTP7	250CTP8	Avg	Min
0	5/8/2024	0	0	2000	2000	2400	1700	1800	1800	1700	1400	1850	1400
1	5/10/2024	23	47	900	2000	1100	1900	1400	1700	1600	1700	1538	900
2	5/13/2024	46	93	1000	1900	1200	1800	1500	n/a	850	1600	1407	850
3	5/16/2024	69	140	1100	1600	1500	1700	1200	1500	800	1400	1350	800
4	5/20/2024	92	186	1100	1600	1300	1300	1400	1400	1050	750	1238	750
5	5/23/2024	138	278	1300	1100	1400	1200	1600	1050	1050	1050	1219	1050
6	5/28/2024	184	371	900	900	1000	900	1300	950	950	900	975	900
7	6/3/2024	268	542	800	850	800	750	950	800	825	825	825	750
8	6/6/2024	314	634	775	675	750	725	775	750	775	775	750	675

Table 14 250 °C coated twisted pair data.

Test #	Date	Time at 250 (hr)	Equivalent Time at 240 C (hr)	PDIV (Vrms)									
				250PTP1	250PTP2	250PTP3	250PTP4	250PTP5	250PTP6	250PTP7	250PTP8	Avg	Min
0	5/8/2024	0	0	2750	2500	2300	2750	2400	2100	2100	2100	2375	2100
1	5/10/2024	23	47	2300	2500	2200	2200	2300	1500	1300	1400	1963	1300
2	5/13/2024	46	93	2200	2400	2000	2400	2300	1400	1200	1200	1888	1200
3	5/16/2024	69	140	800	700	1600	2300	2100	1500	950	900	1356	700
4	5/20/2024	92	186	950	775	1600	1900	2000	675	950	950	1225	675
5	5/23/2024	138	278	775	750	1400	1600	1200	675	1300	900	1075	675
6	5/28/2024	184	371	825	750	1500	1900	2200	700	1000	825	1213	700
7	6/3/2024	268	542	600	700	1200	2300	2100	675	650	800	1128	600
8	6/6/2024	314	634	675	650	1200	2100	1900	650	625	676	1060	625

D. Vendor Wound Motorettes

Two motorettes wound by an outside vendor were tested to complete initial checkout of the thermal cycling rig and obtain information to inform the thermal cycling of the in-house wound motorettes. Figure 42 shows one of the vendor-wound motorettes before potting and Appendix E contains a corresponding drawing.

These motorettes were wound with 25 turns of 25 AWG magnet wire. Eight wires were wound in parallel for each turn. Heavy build MW-16C insulation was maintained for the magnet wire insulation. Coils were wound external to the cores and placed into the slots. A thicker 0.25 mm aramid paper was used for these specimens' slot liner. End boards were made of the same 3D printed nylon with fiber fill material. The end boards were not oversized for the externally wound specimens. As is shown in Figures 42, the externally wound stators have much longer end windings that due not hug closely to the end boards like the windings of the in-house coils. Additionally, the external winding coils overlap significantly in the slots and no gap is present between coils like with the in-house windings. These windings did not meet the desired geometry or specifications for the motorettes. Due to the high number of turns in parallel, it was difficult to separate out wires sufficiently for turn-to-turn PDIV measurements and ensure that the PDIV being measured was within the coil rather than in the lead wires outside of the potting. Phase-to-ground and phase-to-phase PDIV measurements are reported for these specimens.

The first, EM1, was used for initial check out and was cycled with all the machine coils connected in series. Due to the high phase resistance resulting from having all coils connected at once, the current in each coil was limited to 40 A. After some initial checkout cycles, EM1 was cycled between average thermocouple readings of 35 °C and 110 °C. Figure 43 shows example thermal cycle data recorded by the thermocouples on top of the motorette end windings. Figures 44 and 45 show the measured PDIV after different total number of cycles. No notable degradation is shown for any of the phase-to-phase or phase-to-ground PDIV measurements.

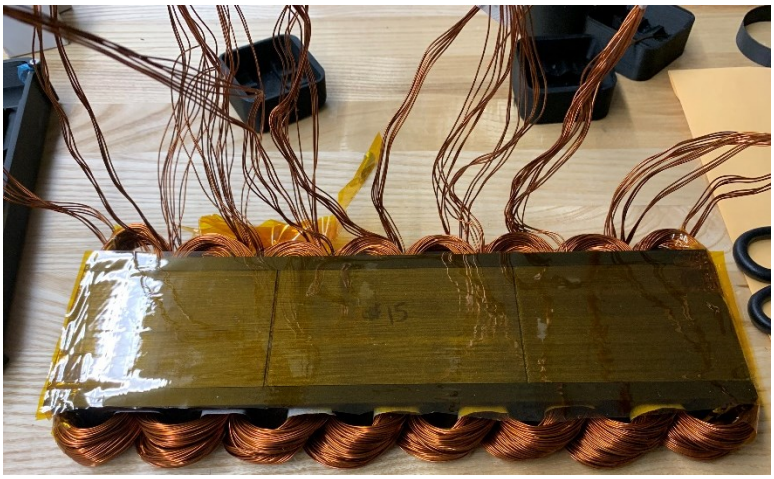

Fig. 42 EM1 prior to potting.

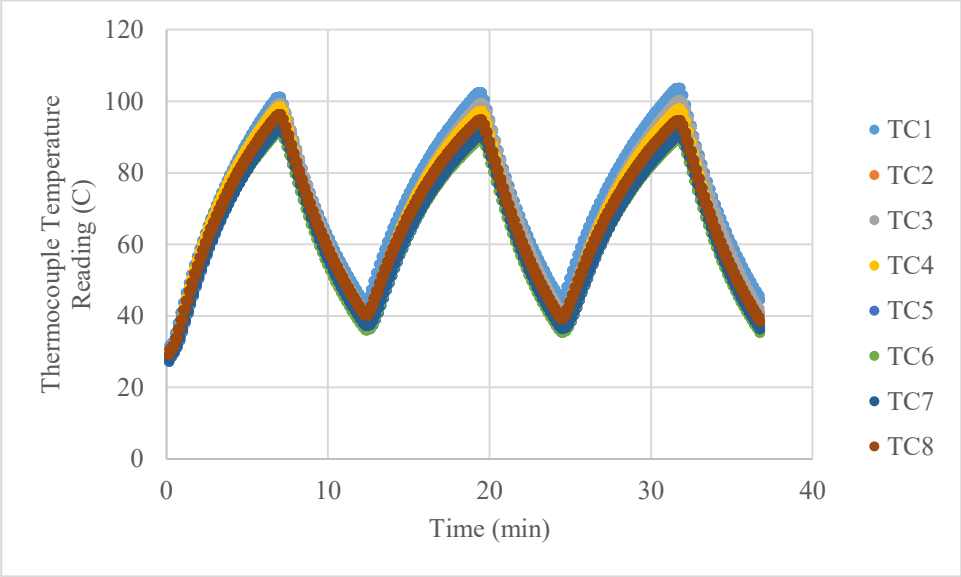

Fig. 43 Example thermocouple temperature readings for EM1.

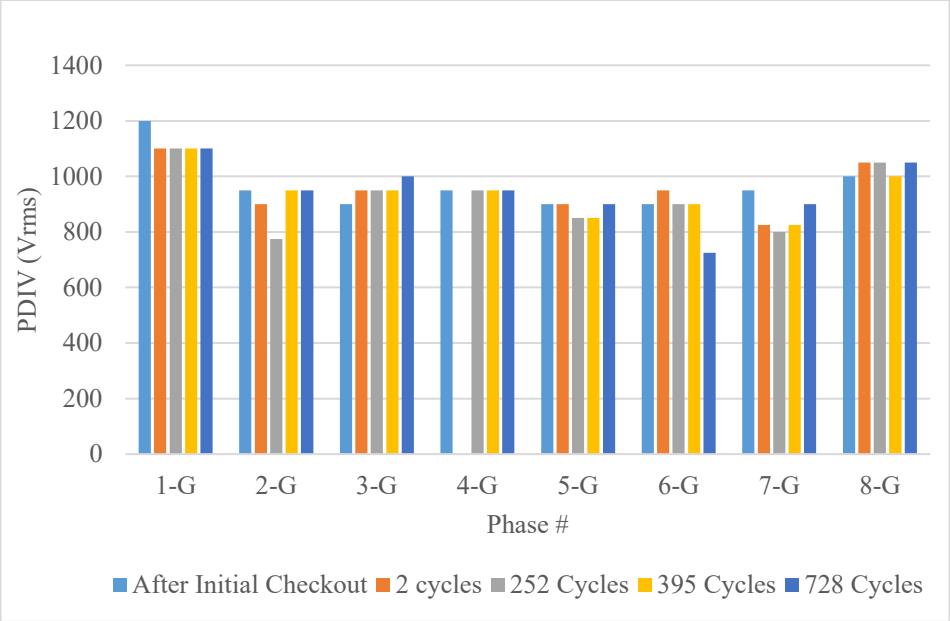

Fig. 44 EM1 phase-to-ground PDIV measurements.

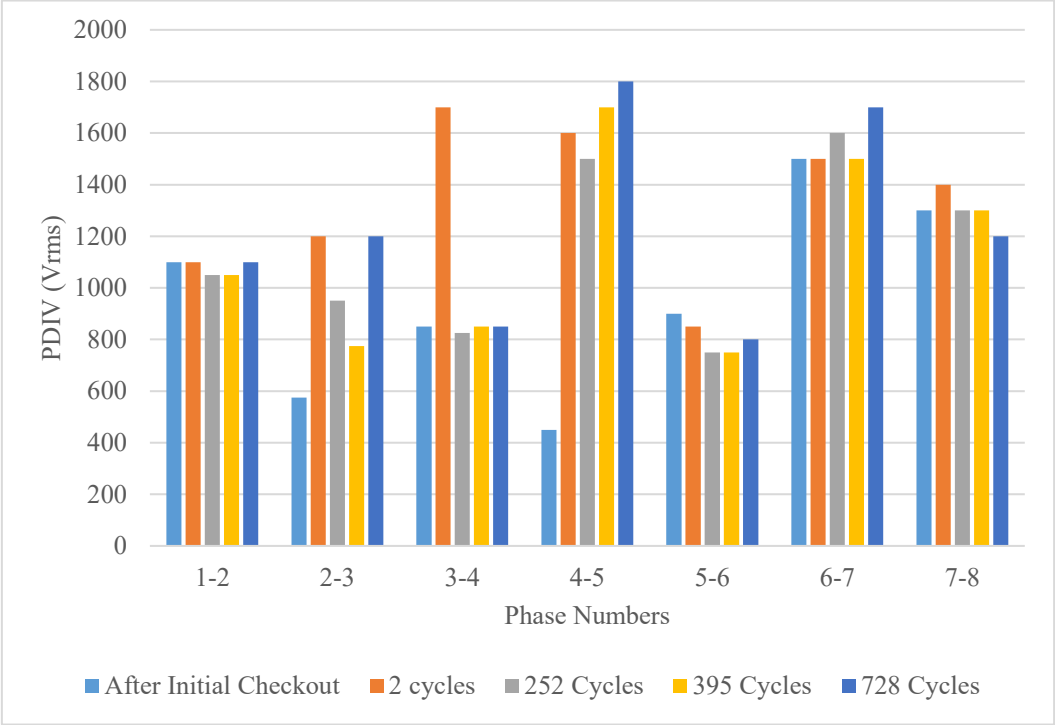

Fig. 45 EM1 phase-to-phase PDIV measurements.

The second vendor wound motorette (EM2) was used to complete a series of single thermal cycles to progressively higher temperatures with PDIV measurements between each cycle. The motorette was then cycled for modest number of cycles at high temperature. EM2 prior to aging had 2 significant defects. The first was a broken phase lead in coil #8, this led to very high temperatures on coil number 7 as coil number 8 received 66% of the current coils 5 and 6 received and coil number 7 received 133% of the current coils 5 and 6 received. The second defect in the motorette was with the end slots for coils 1 and 8. In both locations the loose coil was taped into the slot by the external vendor such that the winding touched the tooth tip without any slot liner between it and the

core's tooth tip. As is shown below, this is believed to have caused the premature failure of the phase-to-ground insulation of coils 1 and 8.

Figures 46 and 47 show the phase-to-ground and phase-to-phase PDIV measurement results for EM2 coils 1 through 4. Coils 1 through 4 were first cycled twice to around 120 °C as a checkout test, then they were cycled once to 140 °C and then to 180 °C with PDIV measured after each cycle. The coils were then cycled 6 times to 180 °C and then 125 cycles were completed to 180 °C. PDIV was measured after each cycling set. In Figure 46, apart from the first coil which had the previously mentioned defect, no significant degradation in phase-to-ground PDIV is visible. In Figure 47, phase-to-phase PDIV degradation can be seen for all phase combinations. The all have decayed by at least 100 V_{rms} with 1-2 having the most degradation at 500 V_{rms}.

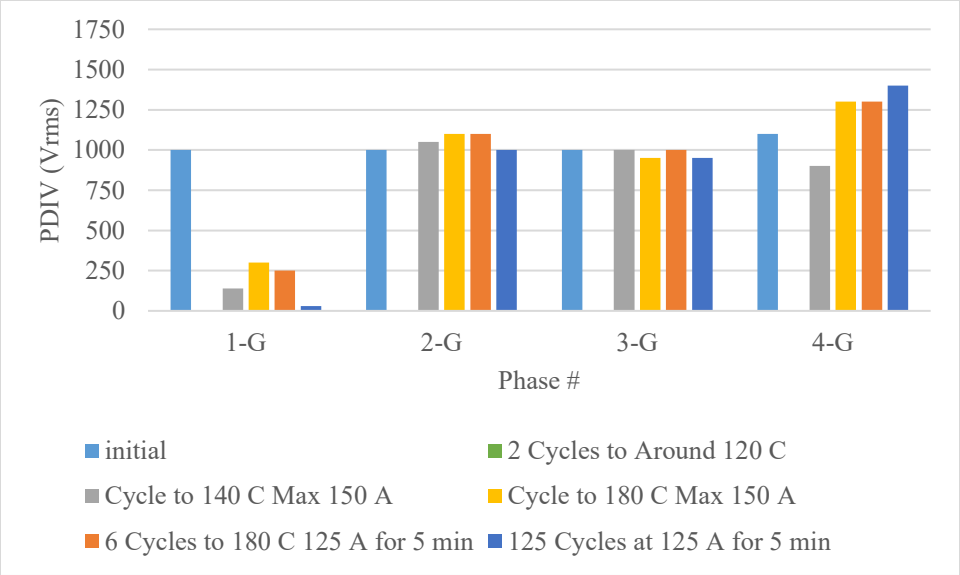

Fig. 46 EM2 coils 1-4 phase-to-ground PDIV measurements.

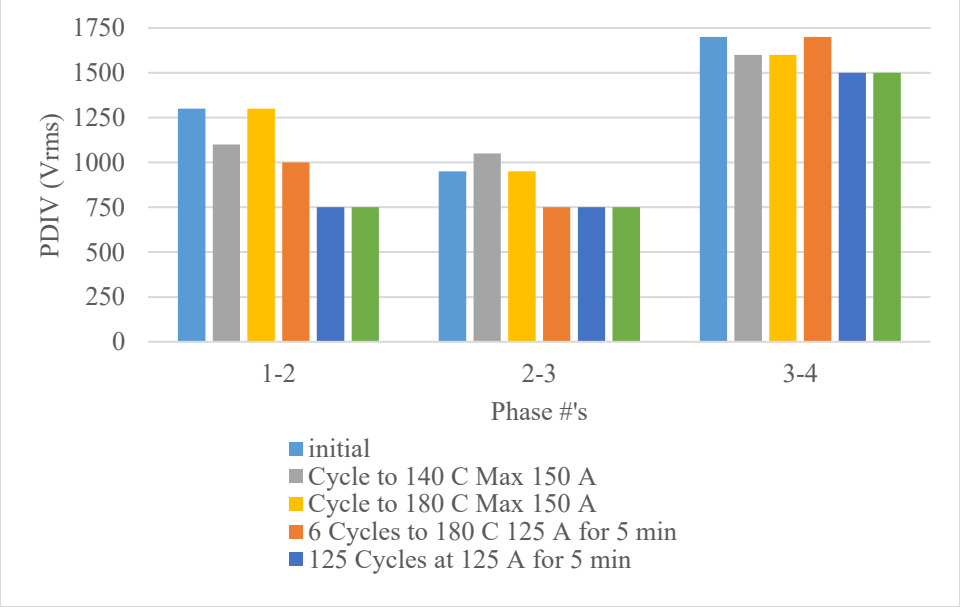

Fig. 47 EM2 coils 1-4 phase-to-phase PDIV measurements.

Coils 5 through 8 were first cycled to 120 °C like coils 1-4. Then they were cycled such that coil number 7 (the one with the most current) got to 220 °C and then 260 °C on its thermocouple readings for single cycles. The coils where then cycled using set currents for set time durations. Five cycles were completed with 150 A for 4.5 min giving coil 7 thermocouple temperatures around 250 °C. Then 87 cycles were completed with 110 A for 6 mins

giving coil number 7 peak temperatures around 260 °C. Figure 48 shows the 5 thermal cycles with 150 A for 4.5 min. Coils 5, 6, and 8 are shown to have similar temperatures significantly below that of Coil 7.

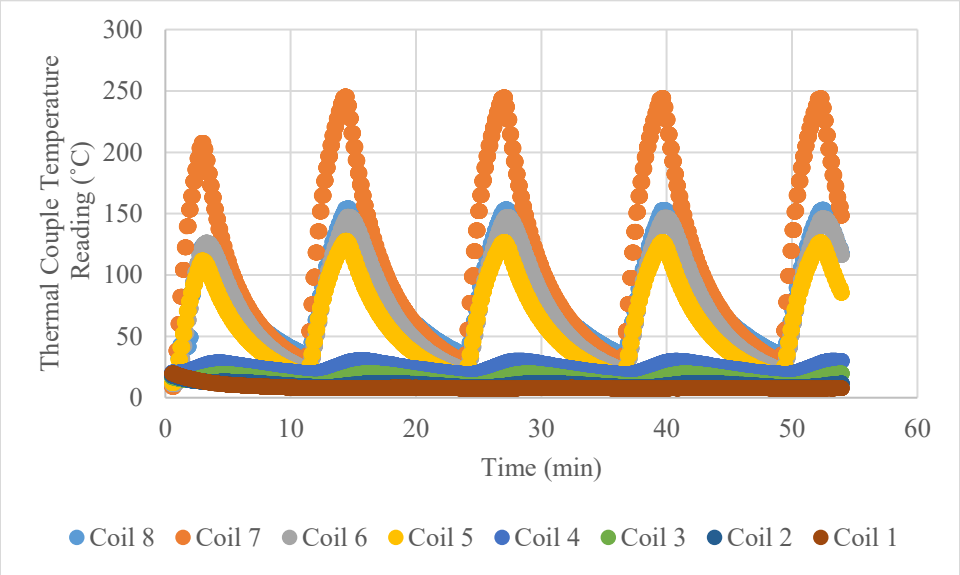

Fig. 48 Example thermal profiles for EM2 coils 5-8.

Figures 49 and 50 show the PDIV measured after each of the cycling runs. In Figure 49, for the phase-to-ground measurements, phase 8 to ground shows significant degradation due to the previously mentioned defect in the phase-to-ground insulation for coils 1 and 8 of EM2. Phase 6 to ground and 5 to ground show no change in PDIV. Phase 7 to ground shows significant degradation of 400 V_{rms} after the 87 cycles to 260 °C. In the phase-to-phase measurements (Figure 50), all phase-to-phase pairs show significant degradation over the cycle count. Phase 5 to 6 shows the most degradation, but also had the highest initial PDIV value. The key conclusion from the EM2 testing was the immediate failure or overly large degradation would not be expected for internally wound motorettes specimens with small cycle counts to temperatures around 200 °C.

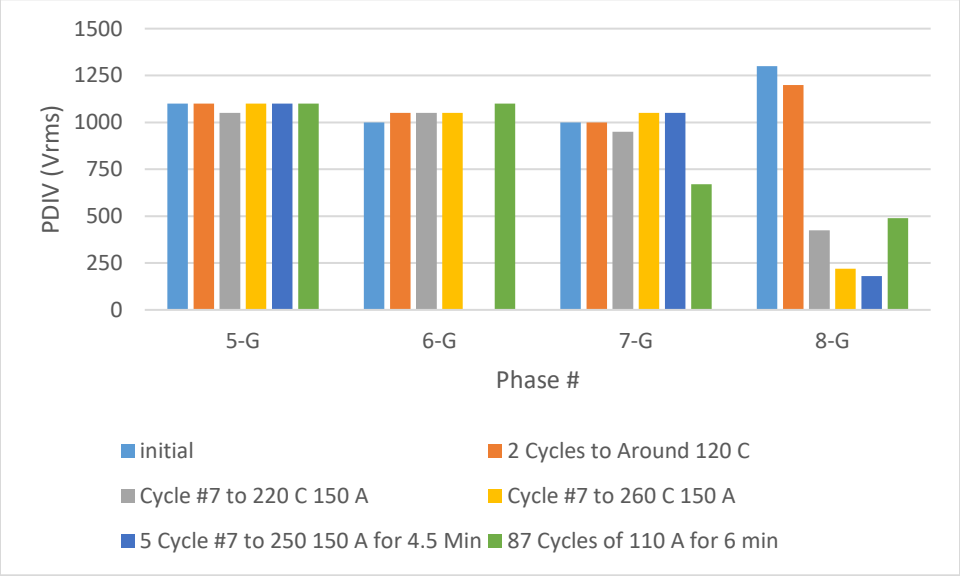

Fig. 49 EM2 coils 5-8 phase-to-ground PDIV measurements.

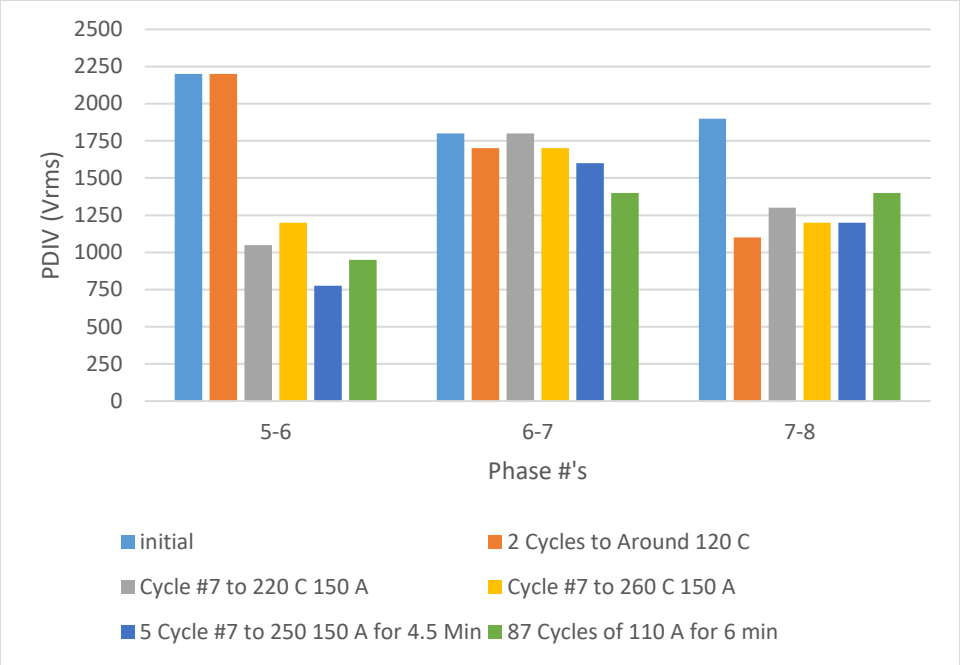

Fig. 50 EM2 coils 5-8 phase-to-phase PDIV measurements.

E. Motorette Drawings

Figures 51 to 53 show the engineering drawings for the motorettes.

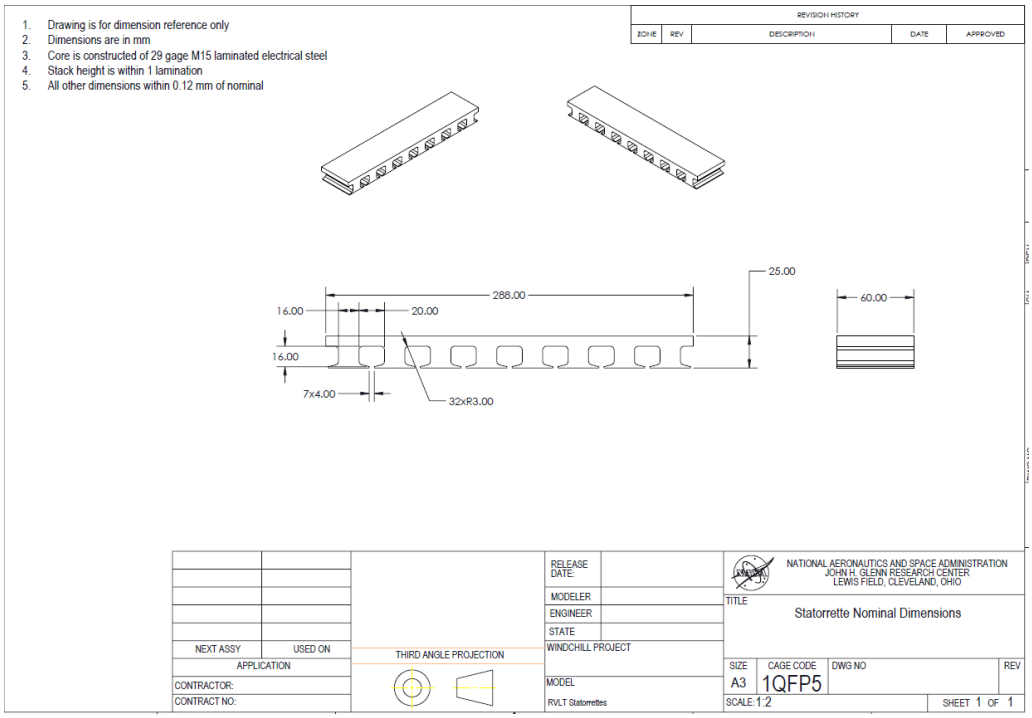

Fig. 51 Motorette iron core geometry.

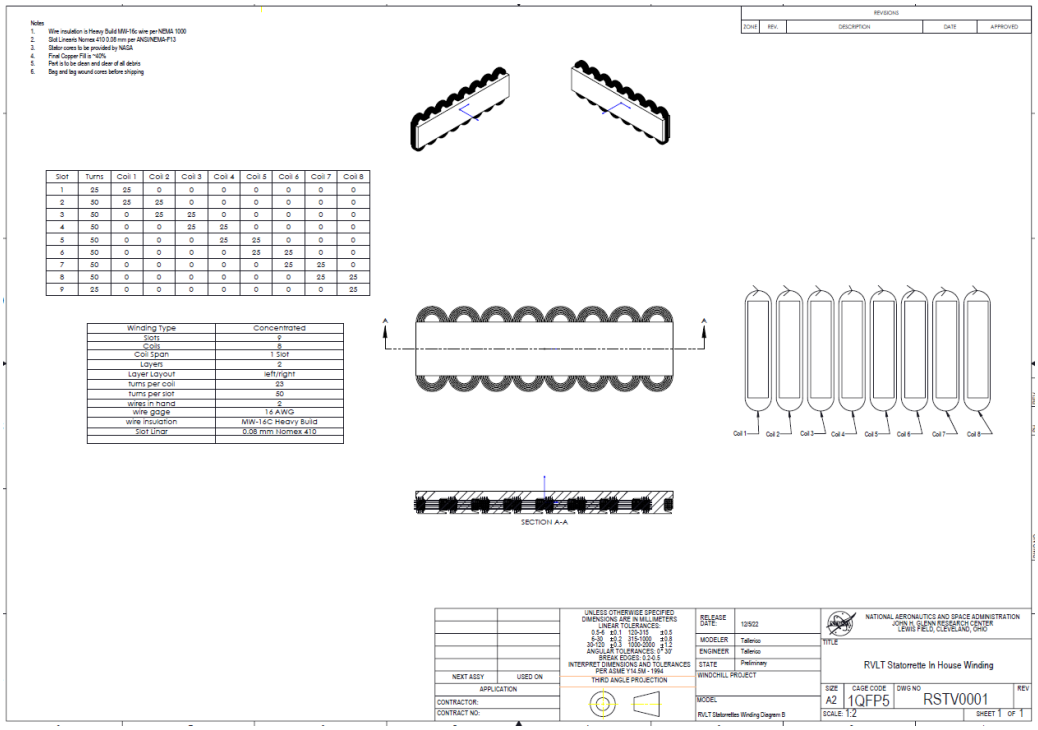

Fig. 52 In-house wound motorette drawing.

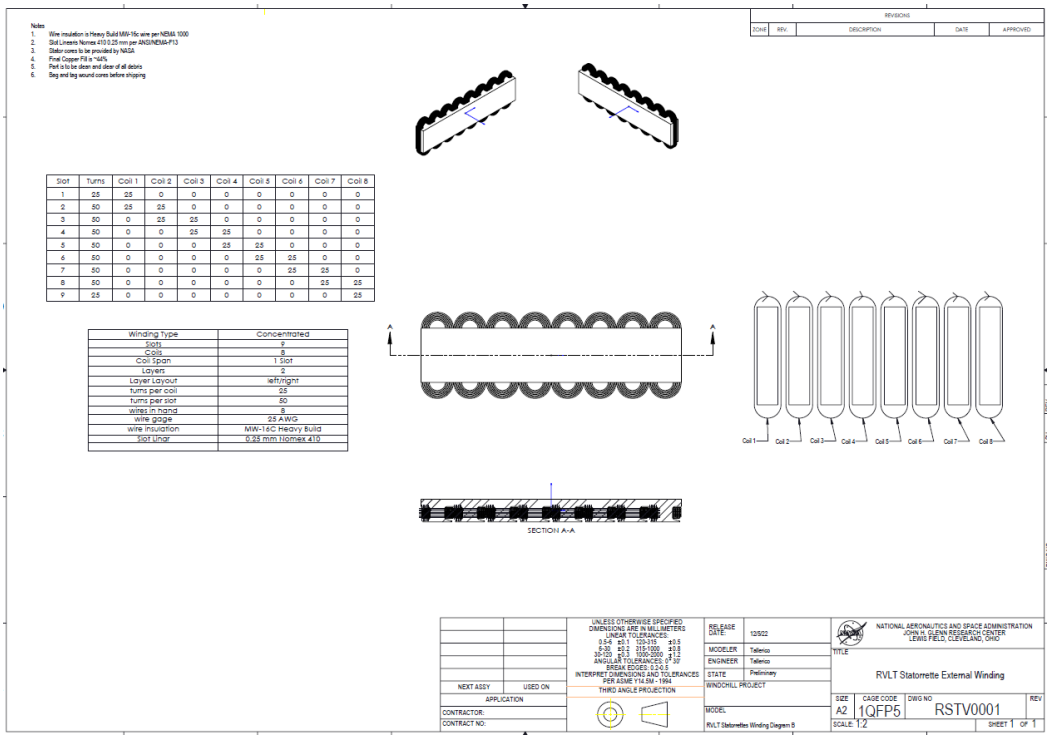

Fig. 53 **Vendor wound motorette geometry.**

F. 3D FEA Model of Thermal Cycling Setup

In order to obtain estimates of the hotspot temperature and the thermal-mechanical stress in the internally wound motorettes during their cycling, a 3D FEA simulation of ¼ of one coil was used. Figure 54 shows the simulation geometry and mesh. All insulation components including the polyimide and Nomex were modeled explicitly. Room

temperature mechanical and thermal properties were used for all components. All materials were modeled as linearly elastic. Heat was applied to the winding based on the current applied in the experiment and the estimated resistivity of the winding based on the temperatures collected by the thermocouples in the experiment. Figure 55 shows the heat load simulated and resulting temperature profiles for Motorette 2. Images of the thermal and mechanical stress results for the full simulation of IM 2 are in Figure 56. The resulting stress in the individual insulation components are in Figure 57.

The thermal simulation is solved for the full transient. The mechanical stress simulation is only solved at the peak temperatures. Stresses reported in Table 4 are evaluated in the polyimide insulation either in the hotspot or as the overall maximum. There is significant difficulty in modeling random wound wires accurately in a finite element simulation. Correspondingly, the stress values reported should be taken as a representative number rather than an explicit estimate of the stress in the insulation components.

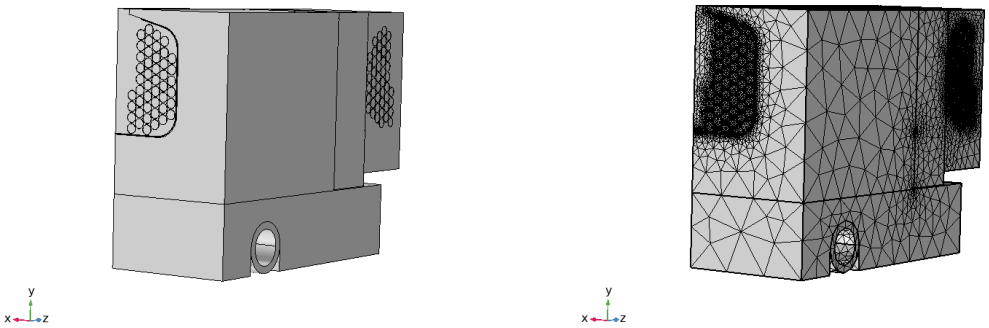

Fig. 54 In-house wound specimen model geometry and mesh.

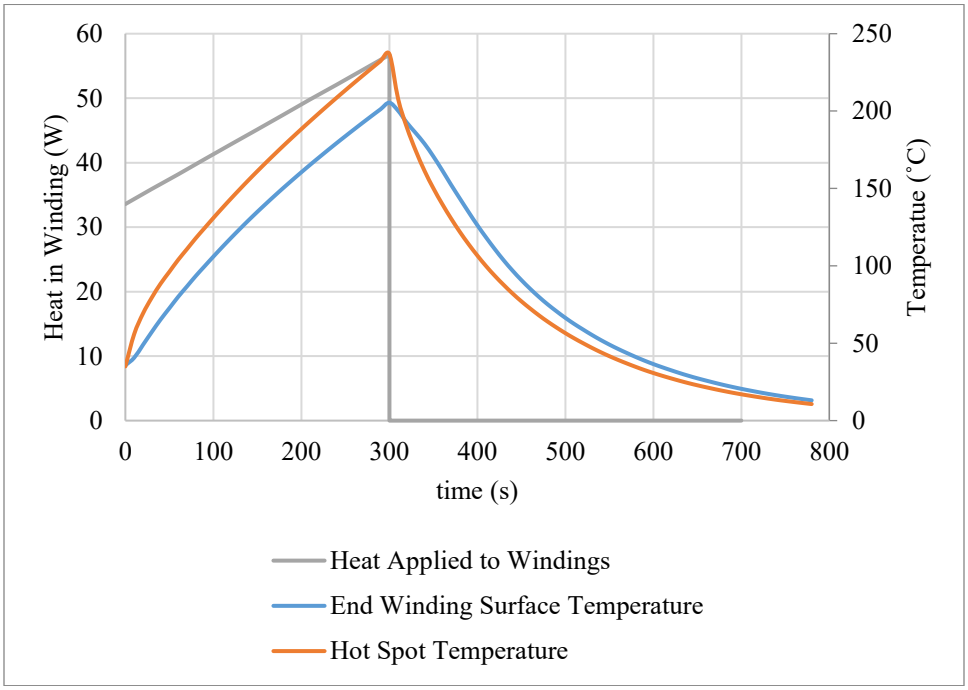

Fig. 55 Example transient thermal profile from FEA model of motorette 2.

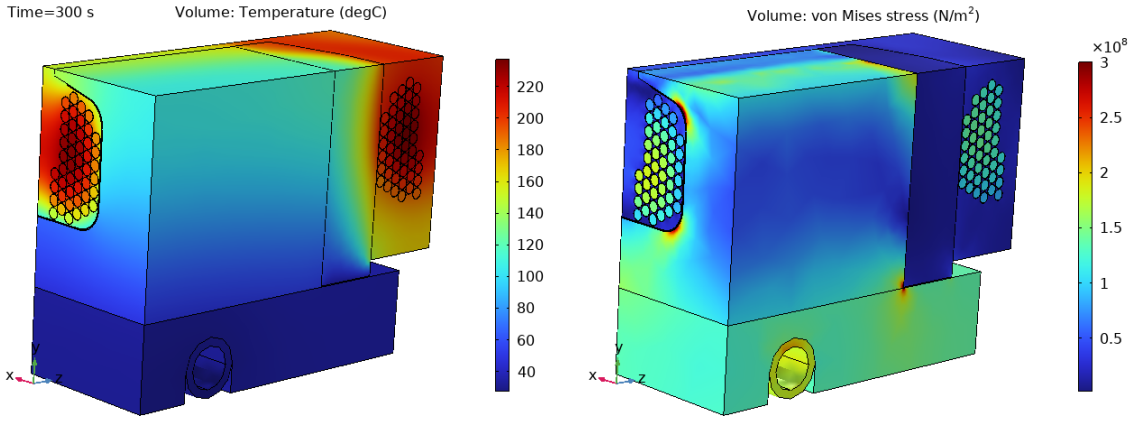

Fig. 56 Winding stress results at peak temperature from Figure 55. Left shows the temperature distribution. Right shows the mechanical stress distribution.

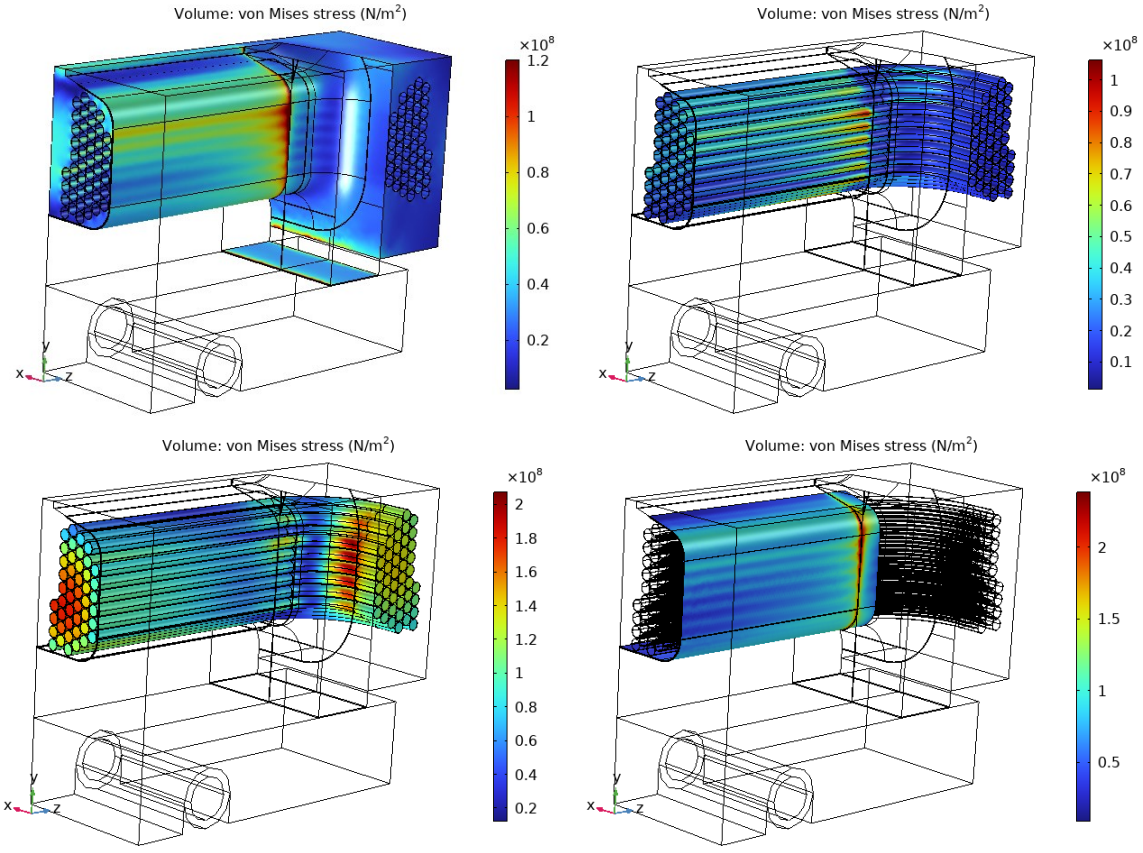

Fig. 57 Simulated Von-Mises stress distributions in motorette 2. Upper left shows the epoxy stress. Upper right shows the polyimide insulation stress. Lower left shows the stress in the copper wires. Lower right shows the stress in the Nomex.

Acknowledgments

The authors would like to acknowledge NASA's revolutionary vertical lift technology and advance air transportation technology projects for funding this work. The authors want to acknowledge Jozsef Puskas, Julius Mirecki, John Veneziano, Acie Rafferty, and Sigurds Lauge for their support building up the experimental setups.

VI.References

[1] P. R. Darmstadt, R. Catanese, A. Beiderman, F. Dones, E. Chen, M. P. Mistry, M. Beckman and R. Preator, "Hazards Analysis and Failure Modes and Effects Criticality Analysis (FMECA) of Four Concept Vehicle Propulsion Systems," NASA, 2019.

[2] T. Tallerico, T. Krantz, M. Valco and J. Salem, "Urban Air Mobility Electric Motor Winding Insulation Reliability: Challenges in the Design and Qualification of High Reliability Electric Motors and NASA's Research Plan," NASA, Cleveland, 2022.

[3] A. Cavallini, "Reliability of Low Voltage Inverter-Fed Motors: What have we learned, perspectives, and open points," in *2017 International Symposium on Electrical Insulation Materials*, Toyohashi, 2017.

[4] T. F. Tallerico, "NASA Reference Motor Designs for Electric Vertical Takeoff and Landing Vehicles," in *AIAA Propulsion and Energy 2021 Forum*, Virtual, 2021.

[5] T. F. Tallerico, J. Chapman and A. D. Smith, "Preliminary Electric Motor Drivetrain Optimization Studies for Urban Air Mobility Vehicles," in *AIAA/IEEE Electric Aircraft Technologies Symposium*, Anaheim, 2022.

[6] F. Loubeau, P. Rain, A. Durieux and F. Le Strrat, "Partial Discharge Behavior of Motorettes Under Different Aging Conditions," *IEEE 2nd International Conference on Dielectrics (ICD),* pp. 1-4, 2018.

[7] A. J. Samarakoon, T. Tallerico, B. Wolhaupter, T. Balachandran and K. Haran, "Partial Discharge Investigation of Electric Machine Winding due to Thermo-Mechanical Stresses for Electric Aircraft Propulsion," in *International Electric Machines and Drives Conference (IEMDC)*, San Francisco, 2023.

[8] P. Mancinelli, S. Stagnitta and A. Cavallini, "Qualification of Hairpin Motors Insulation for Automotive Applications," *IEEE Transactions on Industry Applications,* vol. 53, no. 3, pp. 3110-3118, 2017.

[9] T. Tallerico, M. Hurrell and A. Anderson, "Preliminary Measurements of Partial Discharge Inception Voltage Degradation with Constant Temperature Aging of Magnet Wire Twisted Pairs for Electric Aircraft Motors," NASA, Cleveland, 2023.

[10] International Electrotechnical Commission, "IEC 60270: High Voltage Test Techniques - Partial Discharge Measurements," International Electrotechnical Commission (IEC), 2015.

[11] G. C. Stone, Culbert, Ian, E. A. Boulter and H. Dhirani, Electrical Insulation for Rotating Machines: Design, Evaluation, Aging, Testing, and Repair, Second ed., I. Press, Ed., Hoboken, NJ: John Wiley & Sons, Inc., 2014.

[12] International Electrotechnical Commission, IEC 60034-18-41 Rotating electrical machines –Part 18-41: Partial discharge free electrical insulation systems (Type I) used inrotating electrical machines fed from voltage converters – Qualification and quality control tests, Geneva: IEC, 2019.

[13] L. Lusuardi, A. Cavallini, M. Gomez de la Calle, J. M. Martinez-Tarifa and G. Robles, "Insulation Design of Low Voltage Electrical Motors Fed by PWM Inverters," *IEEE Electrical Insulation Magazine,* vol. 35, no. 3, pp. 7-15, 2019.

[14] A. Rumi, P. Seri and A. Cavallini, "Electric Field Distribution at High Temperatures in Impregnated Enameled Conductors Used in Electrical Machines," in *2023 International Symposium on Electrical Insulating Materials (ISEIM)*, Shimane, Japan, 2023.

[15] Y. Ji, P. Giangrande, V. Madonna, H. Zhang and M. Galea, "Derivation of Ambient Enhancement Factors of Impregnated Twisted Pairs for Partial Discharge Risk Evaluation," *IEEE Transactions on Transportation Electrification,* vol. 10, no. 1, pp. 485-495, 2024.

[16] National Electrical Manufacturers Association, "NEMA MW 1000-2003," National Electrical Manufacturers Association, Rosslyn, VA, 2003.

[17] ASTM, ASTM D2307-2013 Standard Test Method for Thermal Endurance of Film-Insulated Round Magnet Wire, ASTM, 2013.

[18] Dupont, "DuPont Nomex 410 Technical Data Sheet," 2016. [Online]. Available: https://www.dupont.com/content/dam/dupont/amer/us/en/safety/public/documents/en/DPT16_21668_Nomex_410_Tech_Data_Sheet_me03_REFERENCE.pdf. [Accessed 5 June 2023].

[19] Parker LORD Engineering Materials Group, "CoolTherm® EP-2000 Thermally Conductive," 2021.

[Online]. Available: www.lord.com. [Accessed 2023].

[20] A. Rumi, L. Lusuardi, A. Cavallini, M. Pastura, D. Barater and S. Nuzzo, "Partial Discharges in Electrical Machines for the More Electrical Aircraft. Part III: Preventing Partial Discharges," *IEEE Access,* vol. 9, pp. 30113-30123, 2021.